Received: 25 April 2024 | Revised: 24 July 2024 | Accepted: 10 January 2025 | Published online: 18 February 2025

REVIEW

Journal of Optics and Photonics Research
2025, Vol. 00(00) 1–21
DOI: 10.47852/bonviewJOPR52023222

BON VIEW PUBLISHING

Recent Progress in Visible-Light Photocatalysts Materials: Synthesis, Applications, Challenges, and Prospects

Xiaoyang Li[1], Sihan Lin[2], Rongrong Hu[1,*], Pan Liang[3], Qiaoyun Wu[1], Bobo Yang[1], Shengquan Lin[4], Quanlong Xu[5], Junnan Mei[1] and Jun Zou[1,*]

[1]*School of Science, Shanghai Institute of Technology, China*

[2]*The First School of Clinical Medicine, Lanzhou University, China*

[3]*College of Arts and Sciences, Shanghai Dianji University, China*

[4]*Zhejiang Youpon Integrated Ceiling Co., Ltd, China*

[5]*College of Chemistry and Materials Engineering, Wenzhou University, China*

Abstract: Photocatalysis materials have gained significant attention as a powerful tool for environmental remediation and green energy generation, due to their remarkable ability to convert solar energy into chemical energy efficiently. Additionally, photocatalysis also plays a significant role in the medical realm, facilitating advancements in drug synthesis. However, the wavelengths of photocatalysis light normally focus on UV light, which is usually generated by higher energy. In recent years, the spotlight has shifted towards visible-light photocatalysis as a promising green and sustainable alternative due to the increasing concerns about environmental challenges and energy crises. This review focuses on the recent advancements in visible-light photocatalysis materials and emphasizes the diverse types of photocatalytic materials and their impactful applications in environmental remediation, organic synthesis chemistry, and energy conversion. Furthermore, the prevailing challenges and potential solutions in visible-light photocatalysis materials are also summarized to provide valuable insights for the further development and optimization of photocatalysis.

Keywords: visible-light photocatalysis, environmental remediation, green energy, pollution degradation, energy conversion

1. Introduction

The increasing environmental challenges, such as air and water pollution, climate change, and escalating energy crises, imperil both ecosystem balance and human health and set obstacles to sustainable development [1]. Therefore, visible-light photocatalysis has emerged as the most promising candidate, offering energy efficiency and clean reaction conditions without secondary pollution. Through designing material structures, photogenerated electron-hole pairs excited by visible light are separated and directed toward catalytic reaction sites, promoting the chemical transformation of substrate molecules [2]. The applications of visible-light photocatalysis technology are diverse. In environmental remediation, for instance, it could treat air and water pollution [3, 4], reducing environmental stress by efficiently breaking down harmful substances. Furthermore, in energy, it can promote the production of clean energy, such as hydrogen generation [5], thereby contributing to a greener and more sustainable energy landscape. In sum, visible-light photocatalysis offers promising solutions for environmental remediation and clean energy production, illuminating a path toward a more sustainable future.

Many efforts have been dedicated to photocatalysis research, which can track back to scene early 1970s. By using titanium dioxide as a photocatalytic material, water decomposition can be achieved, which paves the way for photocatalysis [6]. Thereafter, in 1976, Carey et al. [7] utilized titanium dioxide to degrade organic pollutants in water, specifically polychlorinated biphenyls. This breakthrough indicated a new era in the application of photocatalysts for wastewater treatment and environmental recovery. In the following, Yokota et al. further expanded the horizons of photocatalysis by demonstrating that TiO_2 exhibits photocatalytic activity for propylene epoxidation under light irradiation. This discovery opened up new routes for organic synthesis, highlighting the diversity of photocatalysis. In 1983, Pruden and Ollis [8] made notable contributions, showing that a range of pollutants, including alkanes, olefins, and aromatics, could be efficiently degraded through photocatalysis. The underlying mechanism of the photocatalytic process is a crucial factor in improving the efficiency of catalysis. Tanaka et al. expatiated the underlying mechanism that hydroxyl radicals (•OH) can drive the degradation of organic compounds. They further

***Corresponding author:** Rongrong Hu, School of Science, Shanghai Institute of Technology, China. Email: hrr92@sit.edu.cn and Jun Zou, School of Science, Shanghai Institute of Technology, China. Email: zoujun@sit.edu.cn

demonstrated that the addition of H_2O_2 could enhance the concentration of •OH, providing valuable insight into optimizing photocatalytic reactions. With the rapid development of industry in the early 1990s, the environmental consequences became increasingly terrible. Among a series of emerging environmental protection technologies, photocatalysis, using semiconductors, driven directly by solar energy emerged as a promising solution for solving environmental pollution. For the first time, the utilization of titanium dioxide photocatalysts for environmental purification was proposed. In recent years, research in visible-light photocatalysis has yielded remarkable advancements. Notably, in 2019, by designing precise nanometer structures, facilitating efficient visible-light catalytic conversion can be successfully achieved. This progress underscores the key role of photocatalysis in tackling environmental challenges and facilitating clean energy production, ultimately providing crucial scientific and technological support for sustainable development.

As a cutting-edge technology in green energy, photocatalysis currently prioritizes research in visible-light photocatalysis, including nanomaterial design, and multi-functional catalytic systems by visible-light-driven. In recent years, the scientific community has been diligently working, aiming to foster environmentally friendly and efficient energy conversion, by enhancing the absorption and utilization of visible light by photocatalytic materials. Despite these advancements, visible-light photocatalysis materials still suffer several challenges, including stability, absorption, catalytic efficiency, selectivity, scale-up production, and regeneration. This paper comprehensively summarizes visible-light photocatalytic materials and applications. Next, the discussion on challenges in visible-light photocatalysis materials is also presented (Figure 1). This review is aimed to serve as a valuable reference, paving the way for enhanced utilization of visible-light photocatalysis, for future research and development.

2. Classification of Visible-Light Photocatalysts Materials

The preparation of high-performance photocatalytic materials holds immense significance in addressing energy challenges, preserving the environment, and fostering sustainable progress, which possess a range of advantageous characteristics, including stability, resistance to photo-corrosion, a wide light response range, a high light absorption coefficient, robust photocurrent density, and superior photoelectric conversion performance. We classify those materials into four main types and summarize their respective catalytic effects in the following.

2.1. Conventional II–VI semiconductor photocatalytic materials

Conventional II–VI semiconductors are of great importance among all the photocatalytic materials. The response mechanism of semiconductor photocatalytic materials during the catalytic process is depicted in Figure 2(a). Upon exposure to light, electrons in the valence band of the semiconductors undergo excitation to the conduction band (CB), resulting in the formation of electron-hole pairs. These highly active electrons and holes can participate in oxidation-reduction reactions with substances adsorbed onto the semiconductor surface, thereby affecting photocatalysis reactions. Specifically, the electrons exhibit a reducing capability, enabling the reduction of organic/inorganic substances adsorbed on the semiconductor surface, while the holes possess an oxidizing ability that can oxidize organic compounds or generate potent oxidizing agents, such as ·OH. ZnS and ZnO are commonly used semiconductor photocatalytic materials. These materials are typically robust in resistance to chemical and photo-corrosion, mild reaction conditions, cost-effectiveness, and low energy consumption. Consequently, they exhibit promising application prospects in water treatment, environmental purification, and renewable energy fields.

The ZnS system has been investigated the most in terms of photophysical processes. Via solvent-free self-overflow strategy, Song et al. [9] introduce DSS (sulfur defects) into ZnS NPs for the production of H_2. As a result, the photocatalytic hydrogen production rate of the defective ZnS can increase up to 21350.23 $\mu mol \cdot h^{-1} \cdot g^{-1}$ ($\lambda = 400$ nm), which is roughly 4.7 times higher than that of pristine ZnS. This result can be attributed to the introduction of DSS, which changes the band position, increases the CB position of ZnS, and enhances the reduction ability of photogenerated electrons. Using a polymer-template self-polymerization method, mesoporous dual-semiconductor ZnS/CdS nanocomposites were synthesized, involving cross-linking polymerization of 5–7 nm-sized CdS and ZnS NPs. Notably, when ZnS content was at 50 wt%, the material achieved an impressive photonic-to-hydrogen conversion efficiency of approximately 60% at 420 nm, along with excellent stability for H_2 generation [10]. Recently, a ZnSe/TiO_2 nanorod heterojunction material was prepared by glancing angle deposition (Figure 2(b)). The fluorine-doped SnO_2 glass and silicon substrates underwent a cleaning process that involved rinsing with acetone, ethanol, and deionized water, subsequently dried with N_2. TiO_2 nanorods were prepared under reduced pressure and in a muffle furnace at 550 °C for annealing before natural cooling to room temperature. ZnSe was layered onto the surface of the TiO_2 nanorods using the same way, without further annealing. Figure 2(b) illustrates substrate rotation speed (n), revolution angle (a), and deposition rate (m) for preparing TiO_2 nanorods and depositing ZnSe on the surface of TiO_2. The variation of ZnSe deposition time determines different samples. When ZnSe was deposited for 100 s, the sample exhibited the highest photocurrent density of about 0.55 mA/cm^2, which was more than double that of pure TiO_2 nanorods. Additionally, it has the best catalytic effect on methyl orange (MO) under visible light for 8 h, with a degradation rate of 45.35% (Figure 2(c)) [11].

However, conventional II–VI semiconductor photocatalytic materials also have several disadvantages in their applications. The capacity to visible-light absorption capacity of conventional II–VI semiconductors, such as ZnS and ZnSe, is relatively limited, which leads to a suboptimal conversion efficiency of solar energy into chemical energy. Besides, the recombination rate of photogenerated electrons and holes in conventional II–VI semiconductor photocatalysts is high. Moreover, some II–VI group materials contain heavy metals such as cadmium, which can pose environmental and health risks.

2.2. The composites of conventional semiconductor and noble metal nanoparticles

Platinum group metal (PGM) nanomaterials, including Au, Ag, or Pt at the nanometer scale, hold revolutionary potential due to their remarkable catalytic properties in environmental remediation and energy conversion. By optimizing shapes and structures and modulating the surface plasmon resonance effects and specific surface areas of PGM nanomaterials, the catalytic activity in photocatalytic reactions can be significantly enhanced [12]. When exposed to light, the surface plasmon resonance effect is triggered,

Figure 1
Classification of visible-light photocatalytic materials, related applications, and challenges

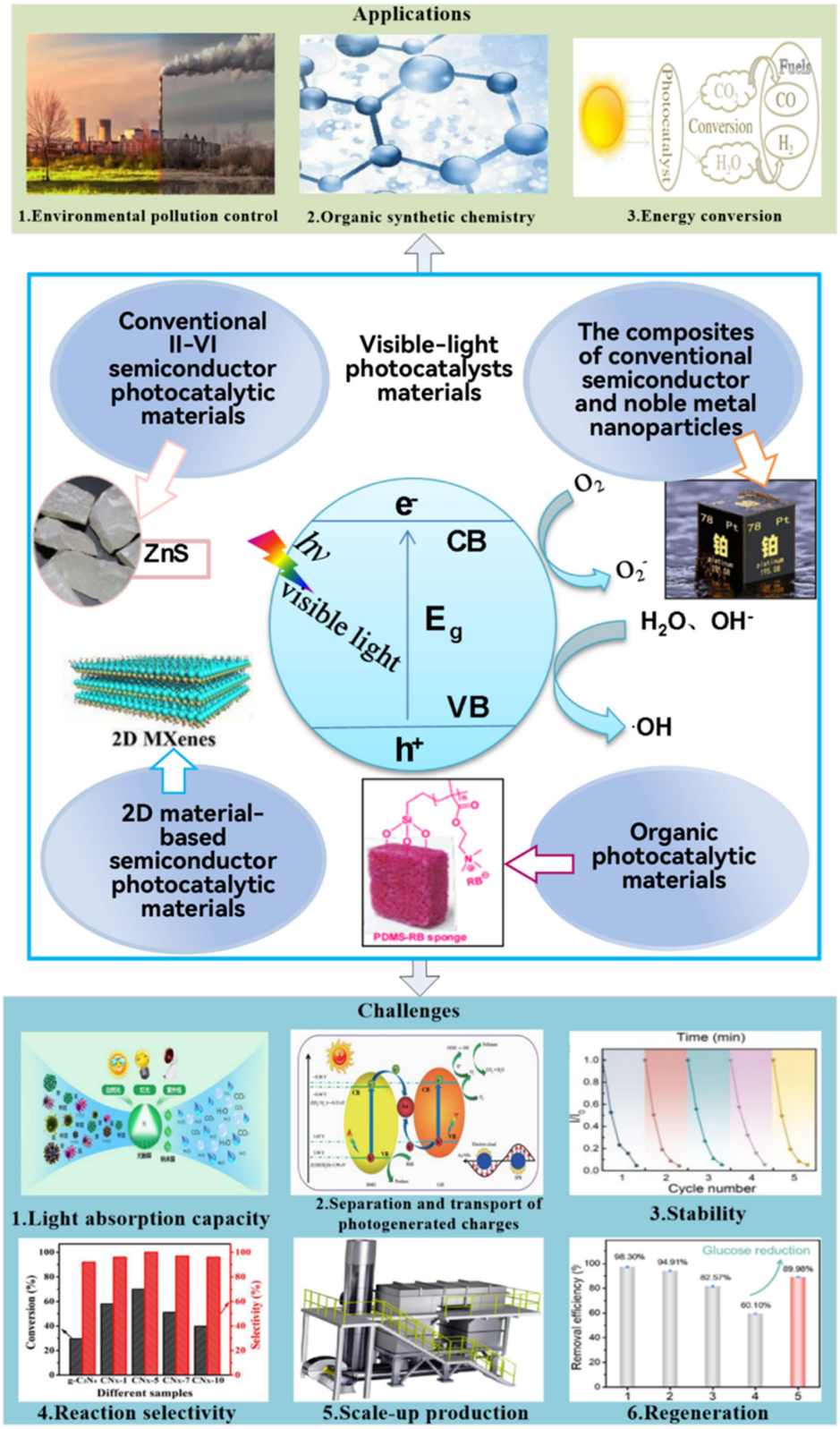

resulting in improved absorption and utilization efficiency of light. This, in turn, enhances the collection efficiency of photogenerated electrons and facilitates the separation and migration of photogenerated carriers, ultimately leading to improved photocatalytic efficiency (depicted in Figure 3(a)). The adjustable nature of PGM nanomaterials, coupled with their excellent catalytic properties, holds promise for a wide range of applications in environmental remediation and energy conversion.

Figure 2
(a) Scheme of photocatalytic mechanism in conventional II–VI semiconductor materials. (b) Preparation flow chart of ZnSe/TiO_2 heterojunction. (c) Photocatalytic degradation curves of MO using ZnSe/TiO_2 nanorod heterojunctions under visible-light irradiation; the inset is first-order kinetics plot of the degradation

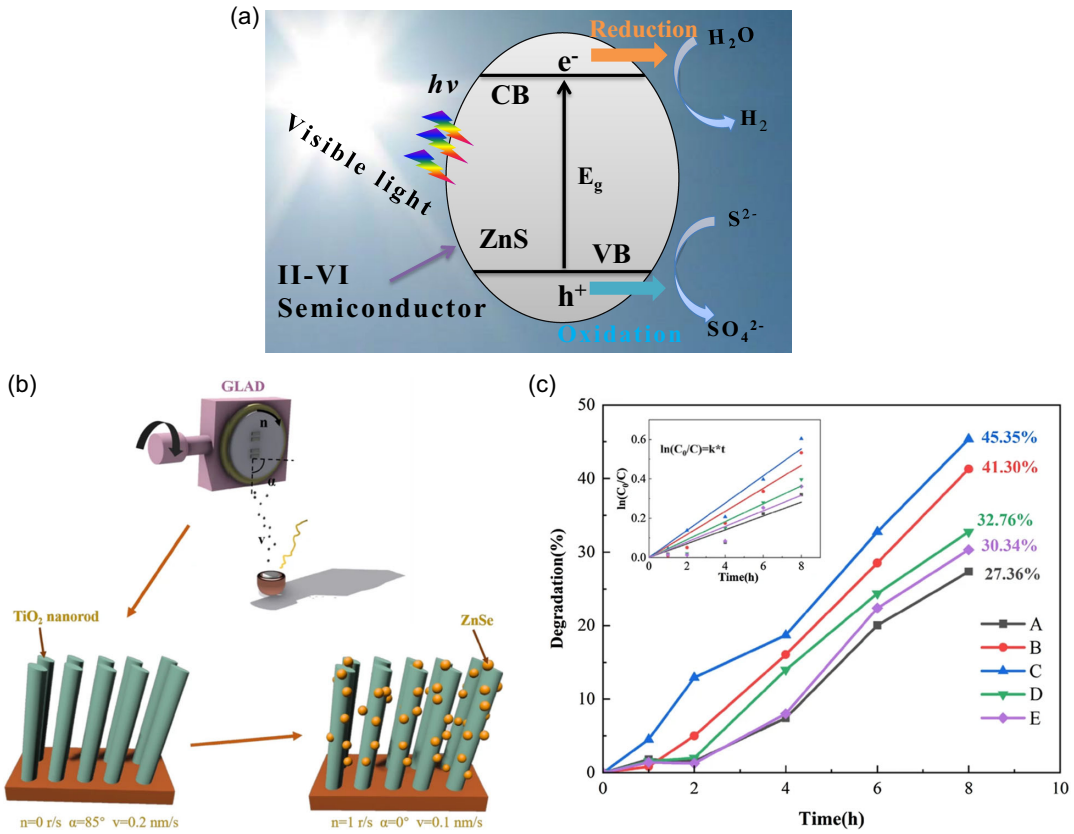

Despite their immense potential in environmental and energy applications, the composites of conventional semiconductors and noble metal nanoparticles face challenges due to high synthesis costs, stability concerns, and limited lifetimes. To solve these issues, many efforts have been made to explore more economical preparation techniques and strategies to enhance the stability of these nanomaterials for practical and reliable application. Gold nanoparticles (Au NPs), when combined with highly dispersed semiconductors, exhibited increased catalytic activity and efficiency [13]. These attributes make them well-suited for photocatalysis, enabling the efficient utilization of light energy to drive chemical reactions. Specifically, the surface plasmon resonance effect in Au NPs can stimulate photons and electrons at the nanoscale, leading to their widespread investigation for photocatalytic pollutant degradation [14]. While TiO_2 is a well-recognized photocatalyst, its performance remains suboptimal due to its limited response to visible light [15, 16]. Via the seed growth method, Au@TiO_2 NPs were synthesized by introducing Au NPs into TiO_2 NPs. The addition of Au NPs induces significant changes to the spectrum of TiO_2. The enhanced activity of core-shell Au@TiO_2 NPs may be due to the improved light-harvesting efficiency based on the resonance of Au ameliorating improved catalytic activity to TiO_2 (Figure 3(b)) [17]. Thus, the integration of Au NPs can significantly enhance the catalytic efficiency of TiO_2.

Ag-NPs are also emerging as promising photocatalysts due to their distinctive optical and electrical properties. The NPs efficiently utilize light energy to drive photocatalytic reactions forward, while also exhibiting robust chemical stability and an extended service lifetime. For instance, using the hydrothermal method, the TiO_2-Ag composites were prepared. The introduction of Ag causes the composite material to exhibit absorbance in the visible-light region (illustrated in Figure 3(c)) [18]. To improve photocatalysis efficiency, the complex of noble metal is a promising way. Using the one pot method, the Ag-Au/ZnO nanocomposites were synthesized. Zinc acetate and polyvinylpyrrolidone were dissolved in ethanol in a round-bottom flask. The mixture was heated to 95 °C until it turned milky-white and then cooled. Chloroauric acid was added for Au deposition, and the mixture was heated to 75 °C for 2 h. The resulting purple Au/ZnO nanocomposites were cleaned and dried. Similar methods were used for ZnO/Ag and ZnO/(Ag-Au) synthesis, with silver nitrate and chloroauric acid added accordingly. In ZnO/(Ag-Au) synthesis, both metal precursors were used at the same time. In comparison with the original ZnO, Ag/ZnO, and Au/ZnO nanosamples, the Ag-Au/ZnO sample showed higher degradation efficiency of MB in visible light (Figure 3(d)) [19].

In summary, the composites of conventional semiconductor and noble metal nanoparticles, including Au and Ag, possess remarkable electrical conductivity and chemical stability. The main mechanism is that these materials induce a surface plasmon resonance effect upon exposure to light irradiation, thus significantly enhancing light absorption and utilization efficiency. Furthermore, these noble metal nanoparticles facilitate the separation and migration of photogenerated carriers, thereby accelerating oxidation-reduction

Figure 3
(a) Schematic diagram of the catalytic mechanism of the composites of conventional semiconductor and noble metal nanoparticles. (b) UV–Vis of AuNPs, TiO_2, and Au@TiO_2 nanohybrids. (c) Photocatalytic MB degradation percentages. (d) Concentration vs time curve for various nanocomposites

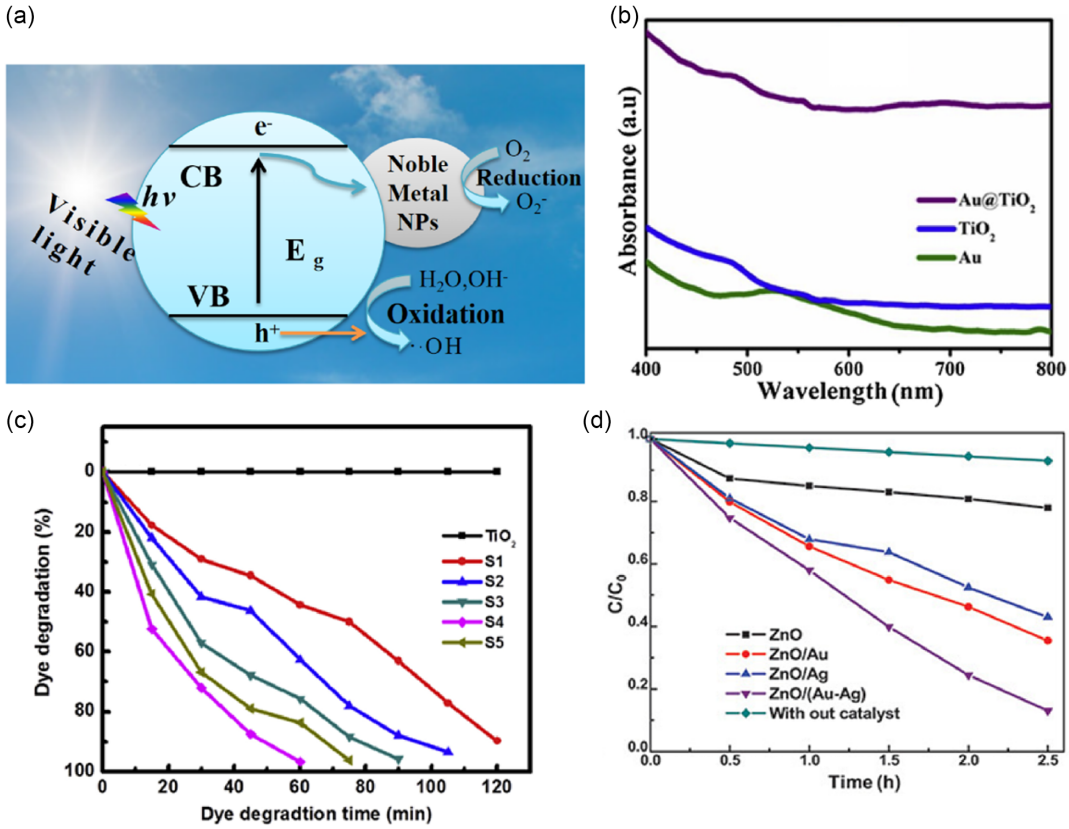

reactions and achieving photocatalytic effects. Importantly, the integration of noble metal nanoparticles enhances the visible-light responsiveness of photocatalytic materials, broadening their range of applications.

2.3. 2D material-based semiconductor photocatalytic materials

The photocatalytic mechanism of those photocatalytic materials based on 2D nanostructures possess planar or layered arrangements is similar to those observed in traditional 3D photocatalysts (depicted in Figure 4(a)), which also can effectively utilize light energy for chemical energy conversion. Notably, 2D materials often exhibit superior surface areas and abundant active sites [20, 21]. Since the groundbreaking discovery of single-layer graphene, 2D materials have triggered significant attention and found rapid application across diverse fields, including photocatalysis [22, 23], energy storage [24], electrocatalysis [25], organic catalysis [26], sensing [27], and magnetoresistance [28]. Alomar et al. [29] used a two-step solvothermal process to craft CdS NPs decorated with MoS_2 nanosheets. The ultrathin MoS_2/CdS nanocomposite, synthesized at 220 °C, exhibited the most remarkable photocatalytic proficiency for MO degradation. Furthermore, this catalyst demonstrated excellent recyclability, maintaining robust catalytic activity even after five consecutive cycles. Utilizing the hydrothermal method, Wen et al. [30] synthesized 2D/2D N-Sn_3O_4/CN-x (x is the percentage composition of N-Sn_3O_4) heterojunction for photocatalytic H_2 production under visible-light irradiation. Photocatalytic H_2 generation rate achieved by N-Sn_3O_4/CN-3 composite stood at a remarkable 1788 μmol h^{-1} g^{-1}, significantly higher than N-Sn_3O_4 (72 μmol h^{-1} g^{-1}) and g-C_3N_4 (1202 μmol h^{-1} g^{-1}). This enhancement was primarily ascribed to the development of an S-scheme heterojunction between the N-Sn_3O_4 and g-C_3N_4 nanosheets, which effectively facilitated the separation and transfer of photoinduced charge carriers. Recently, a 2D graphene oxide (GO) modified α-$AgVO_3$ was synthesized, using a facile in situ coprecipitation method at room temperature. When the content of GO was 0.5 wt%, the GO/α-$AgVO_3$ exhibited the best performance for rhodamine B (RhB) decomposition, with an apparent reaction rate constant 18 times higher than that of pure α-$AgVO_3$ under visible-light irradiation, with a degradation efficiency of 90% and a maximum rate constant of 0.0584 min^{-1}(Figure 4(b) and (c)) [31].

2D photocatalytic materials showed admirable catalytic performance due to their extensive specific surface area, superior conductivity, and exceptional photoelectric properties. Notably, numerous two-dimensional photocatalytic materials are effective under visible-light conditions, as listed in Table 1.

2.4. Organic photocatalytic materials

Organic photocatalysts constitute a class of intricate organic molecules that promote chemical reactions under light illumination. These catalysts possess the remarkable ability to absorb specific wavelengths of light energy and convert it into the

Figure 4
(a) Catalytic mechanism diagram of 2D material-based photocatalytic materials. (b) Photocatalytic degradation curves of RhB. (c) Corresponding pseudo-first-order kinetic curves

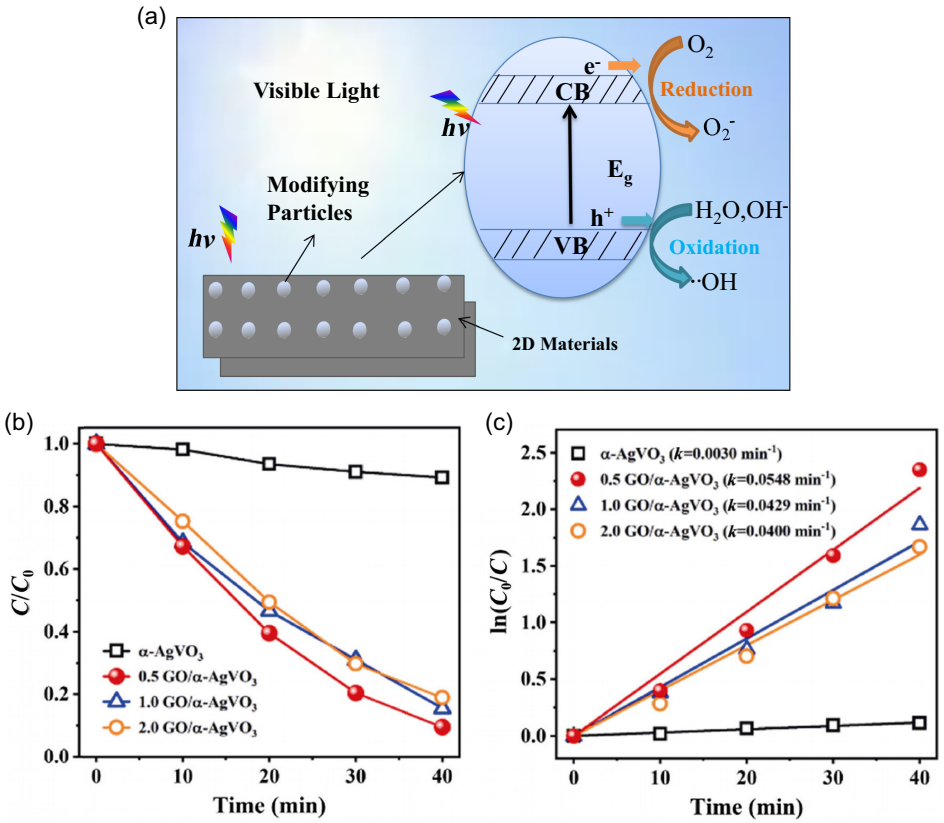

Table 1
2D material-based photocatalysts for visible light

2D material-based composite photocatalyst	Synthesis method	Applications using visible light	Reference
SiP nanosheets	Ultrasound-assisted liquid-phase exfoliation	H_2 evolution	[32]
S-doped and nitrogen-vacant CN	S vapor-annealed CN		[33]
2D/2D CdS/g-C_3N_4 heterojunction	In situ hydrothermal process assisted with microwave	degradation of MO	[34]
SnO_2-nanoparticle-decorated 2D-Bi_2WO_6 nanoplates	Hydrothermal	degradation of RhB	[35]
2D g-C_3N_4/BiOBr heterojunctions	Solvothermal		[36]
Vanadate-rich 2D BiOBr/Bi NSs	In situ preparation		[37]
Ultrathin-layered MoS_2 nanoflowers and nanosheets (NS)	Hydrothermal	degradation of MB, MG, RhB	[38]
2D/2D CoFe-LDH/g-C_3N_4 nanocomposite	Co-precipitation	degradation of tetracycline hydrochloride	[39]
Interfacial coupled TiO_2/g-C_3N_4 2D-2D heterostructure	In situ growth	benzylamine coupling reactions	[40]
2D CoS/BiOBr heterojunctions	Two-step solvothermal route	glyphosate degradation	[41]
2D/2D g-C_3N_4/Bi_4NbO_8Cl nano-composite	Hydrothermal	degradation of oxytetracycline	[42]

required activation energy for chemical transformations, thereby augmenting reaction rates and modifying reaction pathways. Typically, organic photocatalyst materials are characterized by their complex structures, often dotted with chromophores or photosensitive groups that endow them with light-harvesting capabilities. The photocatalytic mechanism primarily relies on the formation of photoexcited states. Upon exposure to light, these organic materials undergo excitation, resulting in the generation of excited states that initiate oxidation-reduction reactions. These reactions are instrumental in the degradation and reduction of

targeted pollutants, underlining the key role of organic photocatalysts in environmental remediation and synthetic chemistry.

Figure 5(a) outlines the intricate reaction mechanism of organic photocatalysts. Initially, the photocatalyst P absorbs light energy, exciting it to the first singlet state ($^1P^*$). This excited state can react with pollutants Q, oxidizing them to $Q^{\bullet+}$ while reducing the photocatalyst to $P^{\bullet-}$. Alternatively, 1P* or its triplet state ($^3P^*$) can interact with water molecules, generating hydroxyl radicals (OH•) and $P^{\bullet-}$. These hydroxyl radicals play a crucial role in oxidizing pollutants. The triplet state $^3P^*$ is also capable of electron transfer reactions with pollutants, forming $Q^{\bullet+}$ and $P^{\bullet-}$. Additionally, $^3P^*$ can react with oxygen to produce singlet oxygen ($^1O_2$). In some cases, the photocatalyst P and pollutant Q form a complex (P-Q) that, upon illumination, undergoes charge separation, generating $Q^{\bullet+}$ and $P^{\bullet-}$. Finally, $P^{\bullet-}$ reacts with molecular oxygen to yield the superoxide anion ($O_2^{\bullet-}$). These various pathways contribute to the photocatalytic degradation of pollutants [43]. This elaborate mechanism highlights the diversity and efficiency of organic photocatalysts in mediating a diverse range of photochemical reactions. These catalysts have found widespread application in the domain of organic synthesis, facilitating reactions such as the formation of carbon-carbon bonds [44] and carbon-nitrogen bonds, acylation, and oxidation-reduction reactions. The significance of sustainable chemical synthesis and green chemistry is immense, as they utilize renewable light energy, thereby mitigating the reliance on traditional, high-energy-consuming heat sources. Recently, molecular organic dye-sensitized photocatalysis materials have gradually emerged as suitable candidates for photocatalysis. Assembling molecular dyes with semiconductors can not only endow them with the conductivity of the semiconductor's CB but also obtain the capability to generate multi-electron carriers through dye excitation. Yang et al. [45] have synthesized a novel material, namely 3D metal-free graphene-organic dye aerogel, via a one-step wet chemical method (depicted in Figure 5(b)). This material significantly enhances the photosensitivity efficiency of molecular dyes and exhibits remarkable catalytic activity towards the photoreduction reactions of nitro compounds and Cr (VI). Furthermore, when compared to graphene-organic powder composites, this graphene-organic aerogel demonstrates superior separation and transfer capabilities for photogenerated electron-hole pairs.

Xu et al. [46] employed both hydrothermal and calcination techniques to synthesize organic porous material-TiO_2/Cu composite materials. Using polydimethylsiloxane (PDMS) sponge as a scaffold (Figure 5(c)), the PMETAC-PDMS sponge was formed through air plasma treatment and vinyltrimethoxysilane

Figure 5

(a) Alternative mechanistic pathways. (b) Schematic (top) and appearance (bottom) illustrations of the preparation of 3D metal-free and robust macroscopic graphene-organics aerogels. (c) Preparation of PDMS-RB (polydimethylsiloxane-Rose Bengal) sponge photocatalyst. (d) The synthetic routes for the furan-based polymers. (e) HERs (hydrogen evolution rates) of the as-synthesized polymers (10 mg) under visible light ($\lambda > 420$ nm)

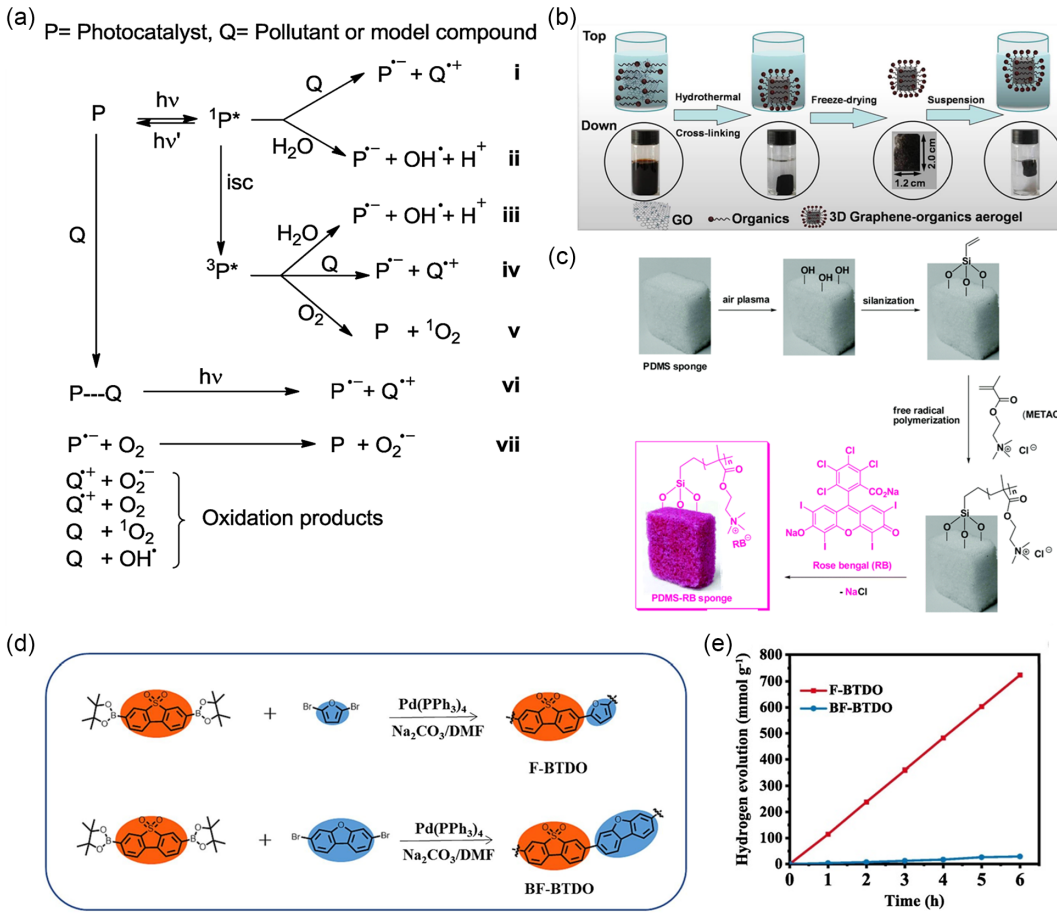

modification, followed by free radical polymerization. Finally, PDMS-RB sponge catalyst was prepared by mixing this sponge with RB salt. This sponge photocatalyst exhibits efficient photocatalytic activity for cross-dehydrogenation coupling reactions under visible-light irradiation and maintains excellent catalytic performance and recyclability even after 15 cycles of use [47]. Recently, two furan-based polymer photocatalysts were prepared, F-BTDO and BF-BTDO, using furan (F) and dibenzofuran (BF) as electron donors, along with dibenzothiophene-S,S-dioxide (BTDO) as an acceptor. The photocatalysts were tested for H_2 production in visible light. As shown in Figure 5(d) and (e), F-BTDO demonstrated higher photocatalytic activity, producing H_2 at a rate of 120.68 mmol h^{-1} g^{-1}, while BF-BTDO exhibited a much lower rate of 4.83 mmol h^{-1} g^{-1} [48].

In summary, organic photocatalytic materials possess the capability to absorb a wide range of spectra, spanning from UV to visible and even near-infrared regions, which enables them to efficiently convert light energy into chemical energy, thereby facilitating photocatalytic degradation reactions of organic compounds. Furthermore, their adjustable structures permit the optimization of photocatalytic performance. The recyclability of these materials contributes to minimizing environmental pollution, thus offering innovative solutions for environmental remediation and beyond. However, the stability of organic photocatalytic materials is relatively poor, and they are prone to photochemical degradation when exposed to light or high temperatures, which limits their photocatalytic performance and lifetimes. Besides, some organic photocatalytic materials may pose biological toxicity or environmental risks.

3. Applications of Visible-Light Photocatalysis

Visible-light photocatalysis has increasingly attracted attention for its applications including environmental remediation, organic synthesis chemistry, and energy conversion. In environmental remediation, visible-light photocatalysis can effectively degrade harmful gases in the air and indoor pollutants, and eliminate various pollutants in the water. In organic synthesis chemistry, visible-light photocatalysis facilitates the production of organic molecules with remarkable efficiency and selectivity, resulting in the generation of high-purity and high-yield organic products. Unlike traditional organic synthesis methods, visible-light photocatalysis eliminates the need for organic solvents and harsh reaction conditions, thereby minimizing environmental impact; in energy conversion, visible-light photocatalysis enables photocatalytic water splitting for H_2 generation and photocatalytic reduction of CO_2, representing a promising avenue for renewable energy production. Additionally, visible-light photocatalysis finds applications in medical fields, optoelectronic devices, and self-cleaning materials, further underlining its diversity and significance. All of those applications not only highlight the potential of visible-light photocatalysis but emphasize its critical role in advancing sustainable development and enhancing the quality of human lives.

3.1. Environmental pollution control

During pollution water treatment, photocatalysis materials, such as TiO_2, can absorb light energy and initiate transformative chemical reactions, which can degrade organic matter, heavy metals, and other harmful pollutants in water. For instance, through photocatalysis, organic compounds such as phenol, dyes, and pesticides can be effectively degraded and converted into safer or more manageable substances. Moreover, this process also exhibits the ability to eliminate microorganisms in water, thereby contributing to the enhancement of water quality.

Wang et al. [49] have presented a type of graphene aerogel (GA) that can effectively remove uranium from water using visible light in air. The GA is made by reducing GO, where the extent of reduction is precisely controlled by temperature. Through experiments, GA-200 (produced at 200 °C) exhibited excellent catalytic performance (Figure 6(a)). Mohsin et al. [50] enhanced the visible-light absorption of ZnO by doping Fe^{3+} and immobilizing it on ceramic plates. This modified material proves highly effective in degrading natural organic matter, particularly humic acid, which offers a promising approach for treating urban wastewater (see Figure 6(b)). In addition, Zhou et al. [51] incorporated the K-g-C_3N_4 photocatalyst into concrete, creating a photocatalytic concrete that exhibits excellent performance in degrading organic dyes in water and visible light (Figure 6(c) and (d)). This innovation holds considerable potential for safeguarding urban water bodies from contamination.

In terms of air pollution control, photocatalysis also has the potential to purify harmful gases in the air, such as nitrogen dioxide, and carbon monoxide. He et al. [52] prepared Ce, S, and N trisubstituted TiO_2 photocatalysts through the sol-gel method with the assistance of ionic liquids. The results showed that the ionic liquids can shift the light absorption area of trisubstituted TiO_2 to the visible-light area. Different types of ionic liquids have different effects. When using 1-butyl-3-methylimidazolium chloride as the ionic liquid, the photocatalytic activity of the composite catalyst is the best and its photocatalytic degradation ability for gaseous toluene is 5.7 times that of naked substituted TiO_2. Table 2 summarizes the parameters of photocatalyst materials in environmental pollution control applications.

Recently, a range of BiOI/SnO_2 heterojunctions (called X%B-S, where X% is the relative amount of BiOI compared to SnO_2, and stands for 15, 30, or 75) were synthesized to efficiently convert NO into NO_3^-. Figure 6(e) shows the preparation of p-BiOI/n-SnO_2 heterojunctions. The heterojunctions were prepared by varying the amount of BiOI to 15%, 30%, and 75% of the SnO_2 weight. Figure 6(f) demonstrates the ability of the newly created catalysts to remove NO. After 30 min, the removal ratio of 30%B-S reached 47.1% under a halogen lamp ($\lambda \geq 420$ nm), and it possessed better stability (Figure 6(g)) [61].

3.2. Organic synthesis chemistry

In organic chemical synthesis, photocatalysis is an essential technique that helps with a variety of reactions, such as coupling and oxidation-reduction processes. The extraordinary selectivity and mild conditions of photocatalytic reactions are their main advantages. The total reaction yield can be increased by these reactions' ability to split or activate particular bonds. Photocatalysis has found widespread application in making pharmaceutical drugs, fine chemicals, and other high-value compounds. Using mesoporous carbon nitride (mpg-C_3N_4) polymer as a semiconductor photocatalyst, combined with its surface alkalinity, can activate O_2 under visible light to highly selectively oxidize benzyl alcohols (BA) to benzaldehyde. It can also selectively convert other alcohol substrates into corresponding aldehydes or ketones [62]. 2,4,6-triphenylpyrylium tetrafluoroborate was also used as an organic photocatalyst by Tambe et al. [63]. Under visible light, molecular oxygen was used as the oxidant to establish a sustainable alcohol oxidation scheme. This scheme achieved the generation of superoxide for the first step of alcohol to aldehyde and singlet oxygen for the second step of aldehyde to carboxylic acid through electron transfer and energy transfer pathways, respectively.

Figure 6

(a) The comparison experiment with different photocatalysts in the removal of uranium. (b) Impact of concentration of HA on the photodegradation ability of ZnO@CP and Fe^{3+}:ZnO@CP. The contrast of concentration of methylene blue (c) under photocatalysis and (d) without photocatalysis. (e) Fabrication procedure of p-BiOI/n-SnO_2 heterojunction. (f) Photocatalytic activity of as-synthesized catalysts for NO removal. (g) stability test of 30 %B-S

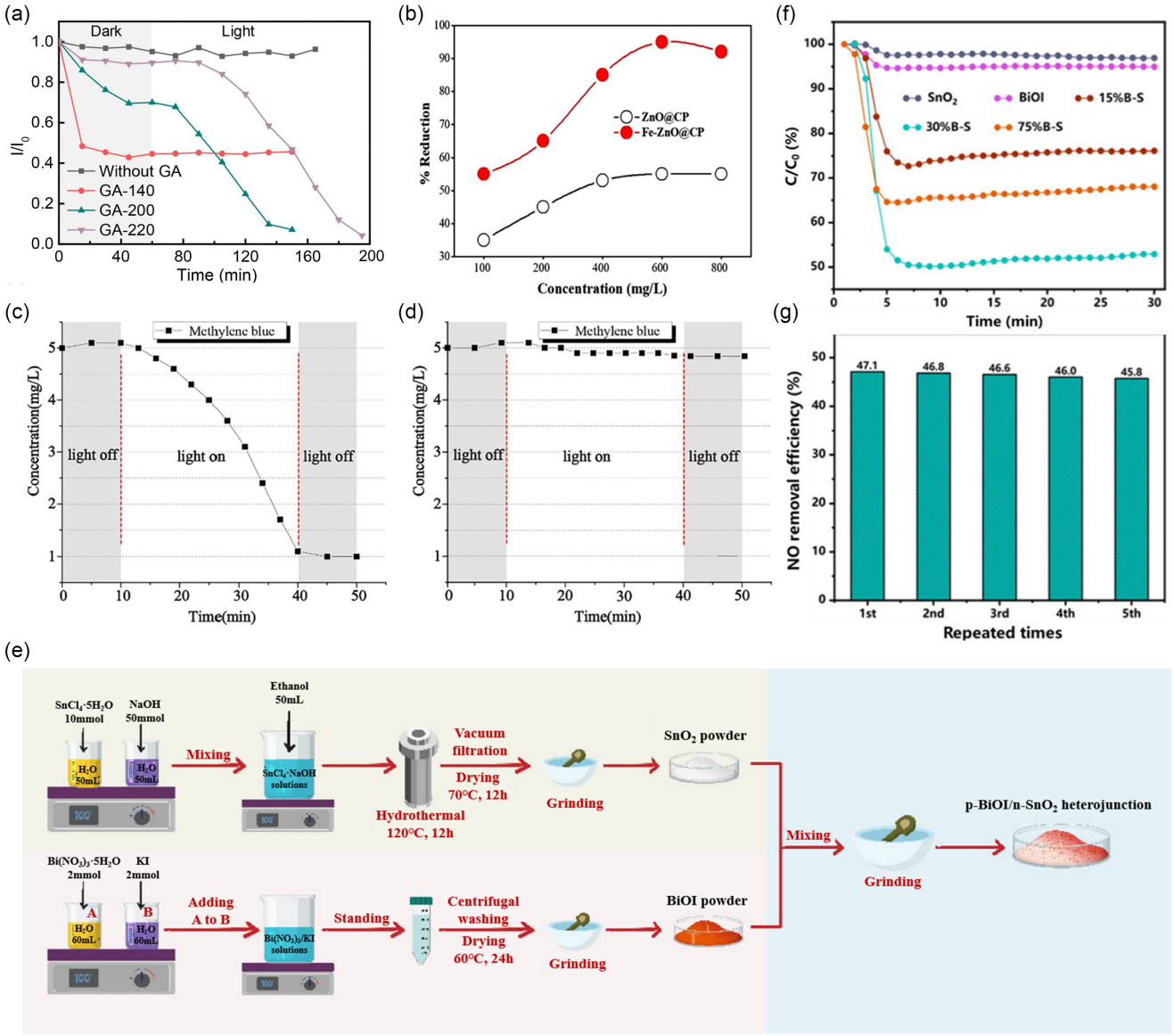

Additionally, the scheme also converted a series of primary and secondary alcohols into corresponding carboxylic acids or ketones and applied optimized reaction conditions to the synthesis of benzocoumarin. Figure 7 shows the mechanism of alcohol oxidation to carboxylic acid. Zhang et al. [64] introduced a new method for allylic silylation reactions using visible light at room temperature. By using an inexpensive organic photocatalyst, they can avoid producing wasteful transition metal salts. Their method also works well for turning silane carboxylic acids into vinylsilanes by removing the carboxyl group.

3.3. Energy conversion

Photocatalysis can not only be applied in environmental treatment and organic chemistry but energy field. The photocatalytic water splitting for H_2 production under visible light provides a feasible solution to energy and environmental issues, which utilizes photonic energy to drive the decomposition of water molecules into H_2 and O_2. Therefore, photocatalysis, especially visible-light photocatalysis, is considered a green and sustainable way of producing hydrogen energy, due to fossil fuel use is not necessary, and the produced hydrogen can be used as a clean energy supply. Xiang et al. [65] used the composite impregnation method to prepare graphene and graphitized carbon-nitrogen (g-C_3N_4) composite photocatalysts. Graphene contents in the samples were varied and labeled GCx (Graphene Content x). The catalytic activities of the composite samples with different GC were evaluated under visible light and their catalytic activities are exhibited in Figure 8(a). It can be seen that the GC has a significant effect on the photocatalytic activity of g-C_3N_4. The Ag_2S/CdS nanocomposites were synthesized through

Table 2
The parameters of photocatalyst materials in environmental pollution control application

Photocatalyst	Photocatalytic performance test	Absorbance peak	Efficiency	Reference
ternary g-C_3N_4/MoS_2/MIL-101(Cr) heterojunction photocatalyst	MO photodegradation	λ = 506 nm	98% (60 min)	[53]
CuS-Fe_3O_4/RGO catalyst	Ibuprofen photodegradation	λ = 496 nm	96% (60 min)	[54]
SnP/AA@ZnO	Amaranth dye photodegradation	λ = 428 and 558 nm	95% (60 min)	[55]
CuO/Bi_2WO_6 Z-scheme heterojunction	Oxytetracycline hydrochloride photodegradation	λ = 424 and 518 nm	86.3% (180 min)	[56]
Bi_2O_2S NS	Congo red photodegradation RB photodegradation	λ = ~496 nm	82% (75 min) 80% (150 min)	[57]
Graphene/ZnO Composite	Ethyl acetate photodegradation 2-Propanol photodegradation Benzene photodegradation	λ = 427 nm	87% (13 h) 83% (13 h) 72% (13 h)	[58]
$GeBu_xH_{(1-x)}$	RhB photodegradation	λ = 800 nm	61% (3 h)	[59, 60]
CNDs/$ZnMn_2O_4$ (20%) nanocomposite		λ = 590 nm	98% (45 min)	

Figure 7
Proposed mechanism of oxidation of primary alcohol to carboxylic acid

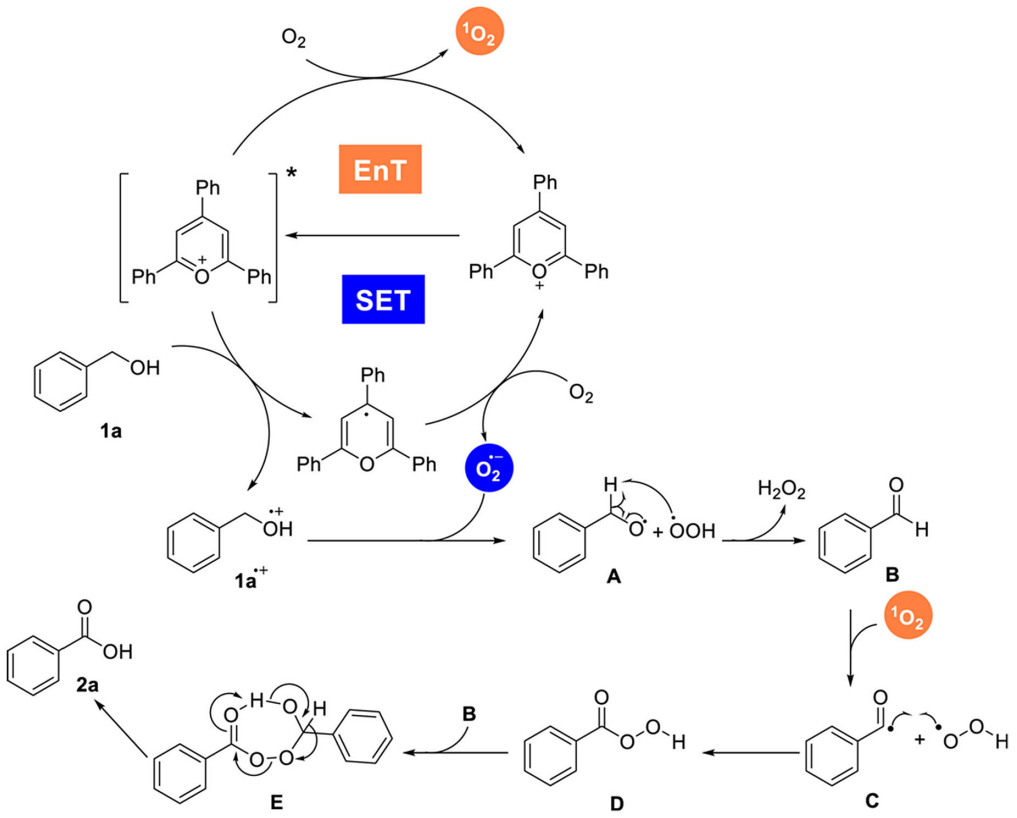

the solvothermal method and subsequent in situ ion exchange method (Figure 8(b)). Figure 8(c) showed the optimal photocatalytic H_2 production rate of the composite material is more than 12 times that of pure CdS. When the Ag_2S content exceeds the optimal value, the H_2 production rate decreases (Figure 8(d)), which is ascribed to the abundant surface H_2 evolution active sites of Ag_2S NPs. When it is excessive, it may cause serious accumulation and shielding of light absorption, leading to a decrease in photocatalytic activity [66].

Guan et al. [67] designed a $PdSe_2$/Sv–ZIS (sulfur vacancies-$ZnIn_2S_4$) semiconductor heterojunction with covalent interface. The sulfur vacancies of Sv-ZIS are filled by Se atoms of $PdSe_2$, leading to the Zn–In–Se–Pd compound interface. The length of the Se–H bond is longer than that of the S–H bond, which facilitates the desorption of H and promotes the production of H_2. As a result, the $PdSe_2$/Sv-ZIS heterojunction demonstrates exceptional photocatalytic performance, achieving a H_2 evolution rate of 4423 μmol $g^{-1}h^{-1}$. Additionally,

Figure 8

(a) Comparison of the photocatalytic activity of the samples GC0, GC0.25, GC0.5, GC1.0, GC2.0, and GC5.0, and N-doped TiO_2 for the photocatalytic H_2 production from methanol aqueous solution under visible-light irradiation. (b) Schematic illustration of the synthesis of Ag_2S/CdS nanocomposites. (c) Time courses of photocatalytic H_2 production, and (d) comparison of the H_2 generation rate of samples over CdS and Ag_2S/CdS nanocomposites under visible-light irradiation. Evolutions of (e) CH_4 and (f) CO with Au-Pt/Cu_2O/ReS_2 samples as the photocatalysts

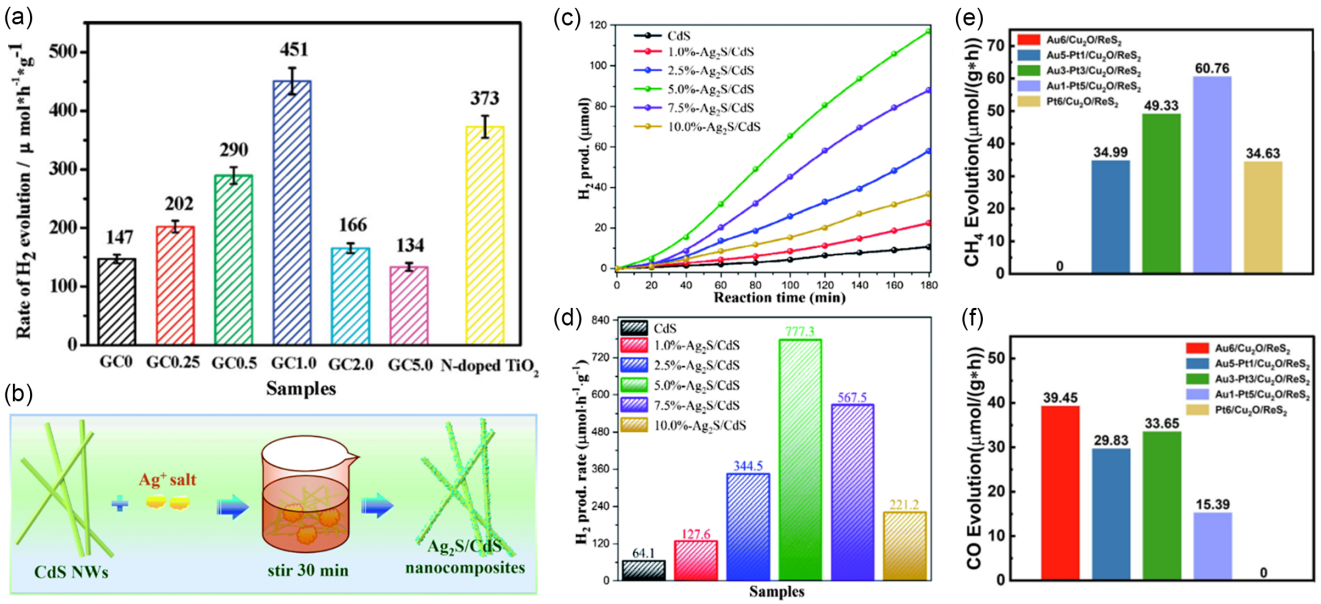

Table 3

The parameters of photocatalyst materials in energy application

Photocatalyst	Photocatalytic performance test	Absorbance peak	Efficiency	Reference
PCCN-20	H_2 evolution	λ = 459 nm	1956.23 μmol g^{-1} h^{-1}	[69]
Ag/TiO_2/g-C_3N_4 nanocomposites		λ = ~425 nm	1.12 mmol g^{-1} h^{-1}	[70]
g-C_3N_4/$KTaO_3$ heterojunction		λ = 426 nm	~842.7 μmol g^{-1} h^{-1}	[71]
2D/2D covalent organic framework/graphitic carbon nitride van der Waals heterojunctions		λ = 620 nm	449.64 μmol h^{-1}	[72]
1D carbon nitride nanotubes	CO_2 reduction	λ = 467 nm	12.58 μmol$g^{-1}h^{-1}$	[73]
CNGA/CdS		λ = 469 and 553 nm	32.75 μmol g^{-1} h^{-1}	[74]
Bi_2WO_6/g-C_3N_4/Cu foam as 3D Z-scheme		λ = ~440 nm	33.84 μmol/g (6 h)	[75]
2D/1D $ZnIn_2S_4$/g-C_3N_4 nested hollow porous heterojunction		λ = 450 nm	79.96 μmol/g (6 h)	[76]

photocatalytic reduction of carbon dioxide is also a research hotspot in the energy field. For instance, the Au-Pt/Cu_2O/ReS_2 photocatalyst synthesized by co-depositing Au and Pt nanoparticles on the Cu_2O/ReS_2 heterostructure can control the selectivity of CO_2 reduction by adjusting the Au/Pt mass ratio, as shown in Figure 8(e) and (f). Under visible light, when the Pt content is 0, CO_2 can only be reduced to CO. Conversely, when the Au content is 0, the reduction product of CO_2 is only CH_4. The Au-Pt bimetallic photocatalyst has a higher yield of CH_4, and the Au1-Pt5/Cu_2O/ReS_2 has the highest yield of CH_4, which is 60.76 μmol/g. This provides significant assistance for photocatalysis in energy conversion [68]. Additionally, the application of photocatalysts in energy is far more than that, and Table 3 shows the results of some researchers. Shortly, photocatalysis will also emerge in the energy field.

4. Challenges for Visible-Light Photocatalysis

With increasingly severe environmental issues and continuous growth in energy demand, visible-light photocatalysis, as a green and sustainable means of energy conversion and environmental protection, has acquired widespread attention. However, in practical applications, visible-light photocatalysis faces challenges such as low light energy utilization efficiency, high recombination rate of photogenerated carriers, and poor catalyst stability. To address these issues, researchers continue to explore and innovate, striving to improve photocatalytic efficiency and stability through methods such as optimizing material structure, surface modification, and preparation of composite materials. The following summarizes the challenges of visible-light photocatalysis in detail, aiming to provide references and insights for related research fields.

4.1. Light absorption capability

UV light only accounts for about 5% of the solar spectrum [77] and may cause certain damage to the human body and biology. Especially in some public places or medical environments, extra safety measures need to be taken to prevent UV light damage to the human body. Therefore, ultraviolet photocatalytic is no longer suitable for the current situation. On the contrary, visible light is a big part of sunlight, making up about 43%, and its impact on biological systems is relatively small, making it more environmentally friendly. Due to the above reasons, visible-light photocatalysis has gradually become a research hotspot in photocatalysis. However, many traditional photocatalytic materials, such as TiO_2, although their light stability and chemical stability enable them to maintain stable physical and chemical properties in various environments, mainly work under UV light and absorb little visible light, which hinders their widespread application in visible light.

Improving the visible-light absorption capability of photocatalytic materials is of crucial importance. Doping and surface modification methods have been proven as effective ways to improve light absorption capability. For example, using a solvothermal method, Ren et al. [78] synthesized HC/BiOCl with the visible-light response by combining biochar (HC) and BiOCl (Figure 9(a)). Under 70 W metal halide lamp irradiation, they degraded RhB. The samples exhibited extremely high visible-light photocatalytic activity (Figure 9(b)). Doping carbon into TiO_2 also could enhance the visible-light absorption capability. As shown in Figure 9(c), the absorption boundary of the composites was transferred to the visible region. Additionally, all the composites exhibited better photocatalytic activity for mercury removal under 24 W white light LED irradiation (Figure 9(d)) [79]. Nowadays, enhancing the light absorption capacity of catalysts remains of most importance. By thermal polymerization, single-atom Ag was anchored on ultrathin CN (UTCN) and the catalyst acquired is called AgUTCN. Firstly, Ag tricyanomethanide (AgTCM) was synthesized by blending $AgNO_3$ and C_4KN_3 solutions at 80 °C. The compound was stirred overnight and the white precipitate was obtained. Then the precipitate was separated, dried, and mixed with dicyandiamide and NH_4Cl to form AgUTCN. After drying and calcination at 550 °C, a light-yellow powder was obtained. UTCN and g-C_3N_4 were also synthesized using similar methods. Figure 9(e) and (f) show how UTCN absorbed and responded to light before and after adding Ag. After adding Ag, UTCN absorbed more light, especially at wavelengths from 450 to 800 nm. Additionally, Ag doping made the material glow brighter at 470 nm when excited with 350 nm light [80]. Although the visible-light absorption capability of photocatalytic materials has significantly improved, it is insufficient for industrial applications, and more research is needed.

4.2. Separation and transport of photogenerated charges

In photocatalytic reactions, the separation and transport of photogenerated charges are crucial steps, affecting the interaction between the catalyst surface and reaction substances and the progress of catalytic reactions. When electrons and holes are excited by light, in some cases they may recombine, so that they cannot be fully utilized in the surface reactions of the catalyst. Additionally, some photocatalysts have limited electron transport distances, especially for materials with poor conductivity or surface structures that are not conducive to electron transport, which limits the ability of photogenerated electrons to transmit within the catalyst to reaction sites and hinders the progress of photocatalytic reactions.

In response to the above two points, it is possible to use materials with good conductivity to dope into the photocatalyst, such as graphene. Graphene doping in photocatalysts like g-C_3N_4 enhances performance, as seen in Xiang et al. [65] where g-C_3N_4 fixed on graphene sheets resulted in over three times the H_2 production rate. Figure 10(a) shows the mechanism of enhanced electron transfer in the graphene/g-C_3N_4 composite material. Additionally, graphene acts as an efficient carrier for photogenerated electrons, reducing electron-hole recombination and advancing photocatalytic reactions, as supported by PL and photocurrent response data. Based on the advancements, recent studies have highlighted the role of photothermal effects in enhancing photocatalytic performance. The integration of photothermal effects, as observed in graphene-based nanocomposites, can substantially increase the separation efficiency of photogenerated charge carriers by converting absorbed light into heat energy. This localized heating accelerates carrier migration, reduces recombination, and thus enhances the photocatalytic process (Figure 10(b)). The photothermal effect can improve the degradation efficiency of organic by ~38%, indicating a promising direction for optimizing photocatalytic material performance [81]. In recent years, ternary Ni_2P/ZIF-8 (zeolitic imidazolate framework-8)/CdS composite was synthesized (Figure 10(c)), which can accelerate the separation of photogenerated carriers. Figure 10(d) presents the photocurrent-time curve, indicating that the introduction of ZIF-8 and Ni_2P significantly enhances the efficiency of carrier separation and transfer in the Ni_2P/ZIF-8/CdS composite. Among the various compositions tested, the 10% Ni_2P/ZIF-8/CdS composite exhibits the strongest photocurrent, demonstrating its superior charge separation and transfer capabilities. Additionally, this composite displays remarkable photocatalytic performance, achieving a high hydrogen production rate of 21.05 mmol g^{-1} h^{-1} and effectively degrading 99% of malachite green under solar light irradiation [82]. Unlike the above methods, via Al reduction in an evacuated two-zone furnace, 2D lateral anatase–rutile TiO_2 phase junctions with controllable oxygen vacancies were fabricated. The 2D lateral phase junctions together with three-dimensional arrays exhibit the highly efficient photogenerated charge separation guaranteed by the build-in electric field at the side-to-side interface. Additionally, the interfacial oxygen vacancies also can further accelerate the separation and transfer of photogenerated charges [83]. In summary, the integration of photothermal effects with traditional photocatalytic mechanisms, along with the strategic design of composite materials and heterojunctions, presents a multifaceted strategy to overcome the limitations associated with charge carrier separation and transport.

4.3. Stability

For practical applications, due to the influence of various uncertain factors, visible-light photocatalytic materials need to have good stability to ensure long-term catalytic activity and recyclability. However, some materials may undergo inactivation and corrosion during photocatalytic reactions, which limits their practical feasibility. TiO_2, for example, is a commonly used photocatalyst, but it easily undergoes lattice defects and surface structural changes under long-term exposure to light, thus reducing its catalytic activity. Therefore, how to improve the stability of catalysts is still a challenge. Using the plasma sputtering method, Ag_3PO_4-GR was synthesized to degrade phenol, which had better stability. The material was prepared in a glass reactor with steel and graphite electrodes, with Ag_3PO_4 sputtered under specific conditions and repeated for 3 cycles. Samples at sputtering times of 15 and 150 s and pure Ag_3PO_4 were tested for stability in four photodegradation cycles. The

Figure 9
(a) UV–Vis diffuse reflectance spectra of samples. (b) Degradation curves of the samples. (c) UV–Vis diffuse reflectance spectra of amorphous C-TiO_2 as-prepared. (d) The mercury removal efficiency. (e) UV-Vis diffuse reflectance spectra. (f) Fluorescence spectra of AgUTCN and UTCN

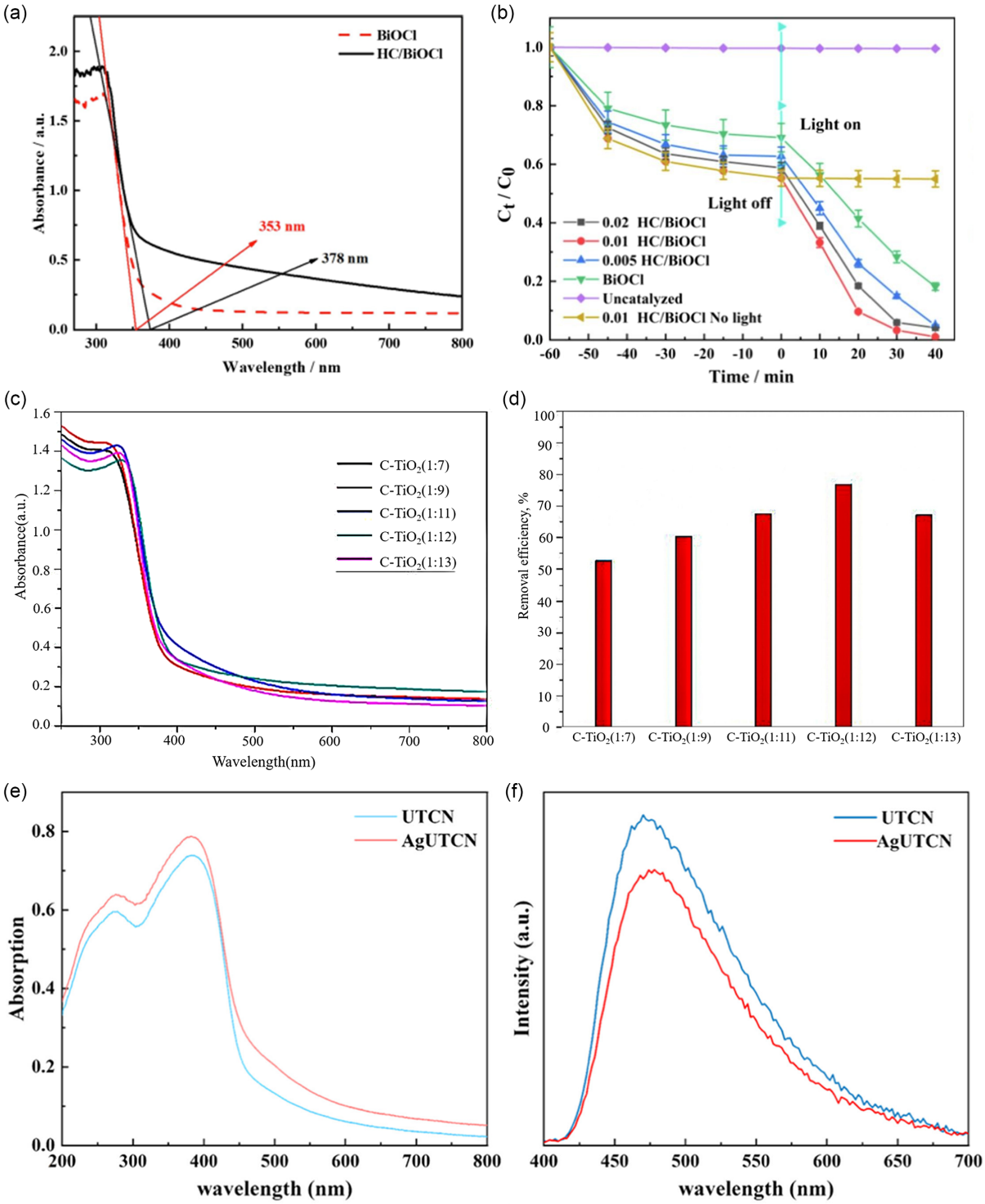

results are shown in Figure 11(a). The stability of Ag_3PO_4-GR (15 s) photocatalyst was significantly improved, while the stability of Ag_3PO_4-GR (150 s) was reduced compared to Ag_3PO_4-GR (15 s), and pure Ag_3PO_4 almost lost its stability. Based on the reaction: $4Ag_3PO_4 + 6H_2O + 12h^+ + 12e^- \rightarrow 12Ag + 4H_3PO_4 + 3O_2$ [84], the primary reason for the instability of Ag_3PO_4 is that photoinduced electrons tend to reduce Ag^+ to metallic silver. Previous experiments have shown that the modification of Ag_3PO_4 by graphene-based nanomaterials can inhibit electron-hole recombination, increase the adsorption of pollutants, and

Figure 10

(a) Enhanced electron transfer mechanism in graphene/g-C_3N_4 composite materials. (b) Mechanism of MB degradation over P25-rGO. Surface plasmon resonance (SPR) under NIR irradiation leads to PTE of rGO. Thermal energy promotes carrier mobility on rGO sheets and thus results in the improved photodegradation activity. (c) Schematic of the formation for the Ni_2P/ZIF-8/CdS composite. (d) CdS, ZIF-8/CdS, 10% Ni_2P/ZIF-8/CdS transient photocurrent response

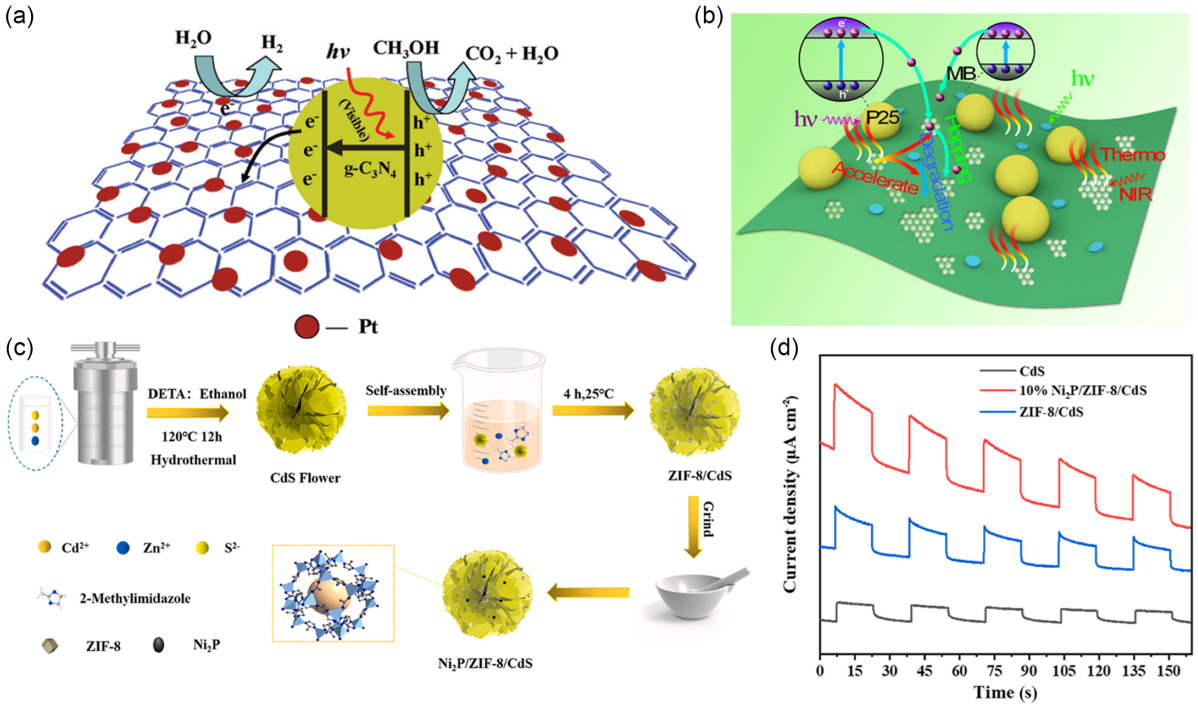

thereby improve the decontamination performance [85]. Graphene or GO can act as electron relays, thereby preventing silver reduction and effectively preventing the above reduction, enhancing material stability. However, the stability of the 150 s sample is not as good as that of the 15 s sample due to the excessive sputtering time that distorts the crystal structure and accelerates silver reduction (Figure 11(b)). Before the process started, only a small amount of silver nanoparticles with a size of about 10 nm were observed. With time, more and more Ag nanoparticles were formed, which affected its stability [86].

The ZnO/Ag/CNT photocatalyst was synthesized by decorating carbon nanotubes (CNT) with Ag and ZnO nanoparticles for the degradation of MB in visible light. The photocatalytic efficiency of ZnO/Ag/CNT was higher than ZnO/Ag and ZnO. This enhanced performance is attributed to the synergistic effects of Ag-NPs and CNT, which facilitate charge separation via Schottky barrier formation at the ZnO/Ag interface and CNT's electron-accepting properties. Besides, repeated experiments have consistently demonstrated the excellent stability of the ZnO/Ag/CNT catalyst as well [87].

4.4. Reaction selectivity

In some complex reaction systems, such as multi-component, multi-step organic synthesis reactions, visible-light photocatalysis often faces challenges in selectivity. In addition to the production of the target product, other by-products such as methane may also be generated. The formation of these by-products not only reduces the selectivity of the catalyst but causes some degree of environmental pollution. Therefore, achieving high selectivity photocatalytic reactions and avoiding the occurrence of side reactions is an important research aspect. For instance, during the experiments on the photocatalytic oxidation of BA to benzaldehyde using porous g-C_3N_4 photocatalyst under the same environment, with oxygen, visible light, and UV light, the selectivity of porous g-C_3N_4 catalysis was greater than 99%. Solvents also affected the selectivity. When acetonitrile was used as the solvent, the selectivity of benzaldehyde decreased to 68% [88]. The introduction of nitrogen vacancies (NVs) into g-C_3N_4 enhances its photocatalytic performance for selective oxidation of BA to benzaldehyde. Theoretical calculations indicate that NVs promote the adsorption and activation of oxygen molecules, while experimental results show that nitrogen-deficient g-C_3N_4 (CN-x) exhibits significantly higher conversion efficiency and product selectivity compared to pristine g-C_3N_4 under visible-light irradiation (Figure 12) [89]. Despite some progress in improving selectivity, further enhancements still require additional research.

4.5. Scale-up production

Some advanced photocatalytic materials synthesis methods are complex and expensive, making it difficult to achieve large-scale preparation and limiting their practical application. In addition, the reaction conditions of photocatalysis are relatively harsh, requiring specific light, temperature, and pressure conditions. These conditions may increase production costs and limit their popularity in industrial applications.

The new concept of intermolecular charge transfer for photoredox catalysis based on visible-light excitation was proposed. Besides, a simple, efficient, and environmentally friendly non-metal anion

Figure 11
(a) Stability experiment results. (b) TEM images of Ag_3PO_4-GR (150 s) before and after the photocatalytic degradation of phenol in (a–c) and (d–f)

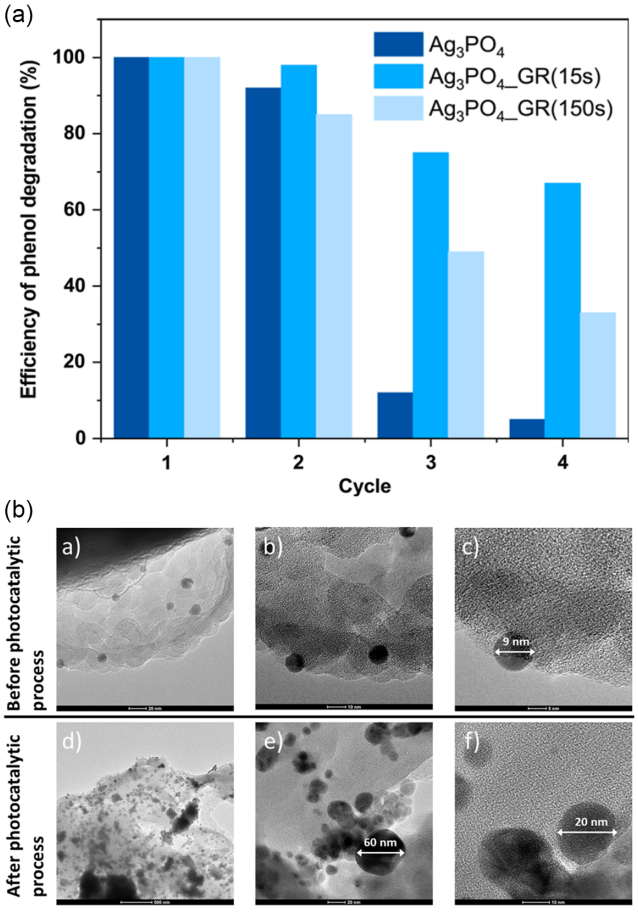

Figure 12
Photocatalytic selective oxidation of BA on different catalysts

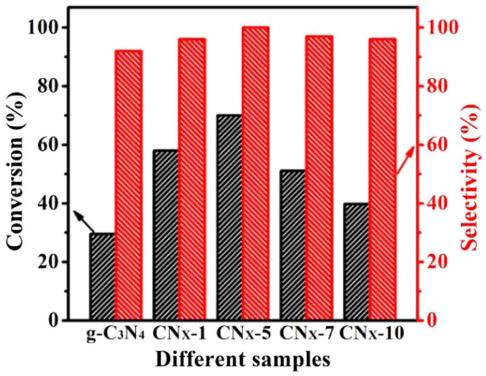

complex photocatalytic system was discovered that uses inexpensive sodium iodide, triphenylphosphine, and carboxylate as raw materials to successfully achieve the decarboxylation reaction of fatty carboxylic acid derivatives. Most importantly, this type of catalytic system can maintain high catalytic efficiency when the production reaches gram-scale quantities, indicating its potential for industrialization [90]. Ma et al. [91] used the coprecipitation method to synthesize photocatalysts of phosphorus compounds/CdS for hydrogen production. After loading CoP and MoP catalysts, the hydrogen production increased significantly. The CoP/CdS and MoP/CdS systems achieved optimal hydrogen production rates of 140 and 78 μmol/h, respectively, exceeding CdS by 7.0 and 4.0 times and Pt/CdS by 2.0 and 1.1 times (Figure 13(a)). This suggests that CoP and MoP, as cost-effective non-noble metal catalysts, exhibit remarkable photocatalytic activity for H_2 production, making them viable alternatives to noble metals. Large-scale hydrogen production becomes feasible with such catalysts. Efforts to synthesize materials with precise control over molecular weight and dispersity for industrial applications are ongoing. Fang et al. [92] developed a PPh3-CHCP photocatalyst using a phosphine-based conjugated hypercrosslinked polymer. PPh3-HCP was synthesized via Friedel-Crafts alkylation between TPP and DMB with $FeCl_3$, followed by reduction with $NaBH_4$ to yield PPh3-CHCP (72.5% yield). This photocatalyst enables efficient, large-scale Cu-ATRP, achieving monomer conversions close to 99% for various monomers at a 200 mL scale and enabling the synthesis of block copolymers at a 400 mL scale (Figure 13(b) and (c)). However, there is still a need for the preparation of diverse visible-light photocatalysts and the enhancement of their performance for industrial applications, which requires further research efforts.

4.6. Regeneration

The regenerative capacity of photocatalysts is an essential aspect of their practical application, directly relating to the catalyst's lifespan and economic viability. The process of photocatalyst regeneration aims to restore their catalytic activity, allowing for reuse across multiple reaction cycles. However, the regeneration process itself faces a series of challenges, including issues of regenerative efficiency, cost, environmental impact, and operational complexity. Therefore, understanding and optimizing the mechanisms of photocatalyst regeneration is crucial for advancing the field of photocatalysis. We will now delve into two primary mechanisms of photocatalyst regeneration: photoreduction and chemical reduction. Photoreduction utilizes photogenerated electrons to reduce oxidized catalytic species back to their active state. For instance, in the TiO_2 nanotube-based catalyst (TNT(Pd)/Fe_2O_3), Pd nanoparticles generate photoelectrons that rapidly separate and traverse the TiO_2 wall to the Fe_2O_3 surface, reducing Fe^{3+} to Fe^{2+} and continuously regenerating the most active Fe^{2+} sites for the Fenton reaction. After several cycles (Figure 14(a)), the MO degradation performance under photo-Fenton catalysis showed no decay, demonstrating the self-regeneration of Fe^{2+}, with a slight increase in the number of Fe^{2+} species revealed by XPS measurements post-long-term stability tests (Figure 14(b)) [93]. Chemical reduction, on the other hand, involves the use of reducing agents to restore the catalyst's active state. For example, in the Cu_2O/BiOBr S-scheme heterojunction photocatalyst, glucose acts as a reducing agent capable of reducing Cu(II) back to Cu(I), thus achieving catalyst regeneration. As shown in Figure 14(c) and (d), the photocatalytic degradation efficiency, which dropped to 60.10% after four cycles, was significantly restored to 89.98% with the addition of glucose, demonstrating the effectiveness of this method in regenerating the used catalyst [94]. The combination of these two mechanisms, that is, the synergistic effect between photocatalysis and Fenton-like reactions, provides a strategic approach to enhancing the overall performance of photocatalysts. In the TNT(Pd)/Fe_2O_3 system, the synergistic

Figure 13
(a) Comparison of photocatalytic activities of sulfides/CdS with CdS and Pt/CdS. (b) Strategy for the fabrication of PPh3-CHCP photocatalyst. (c) Photoinduced Cu-ATRP in the presence of PPh3-CHCP (inserted photo: 200 mL reaction scale of PMA under sunlight irradiation)

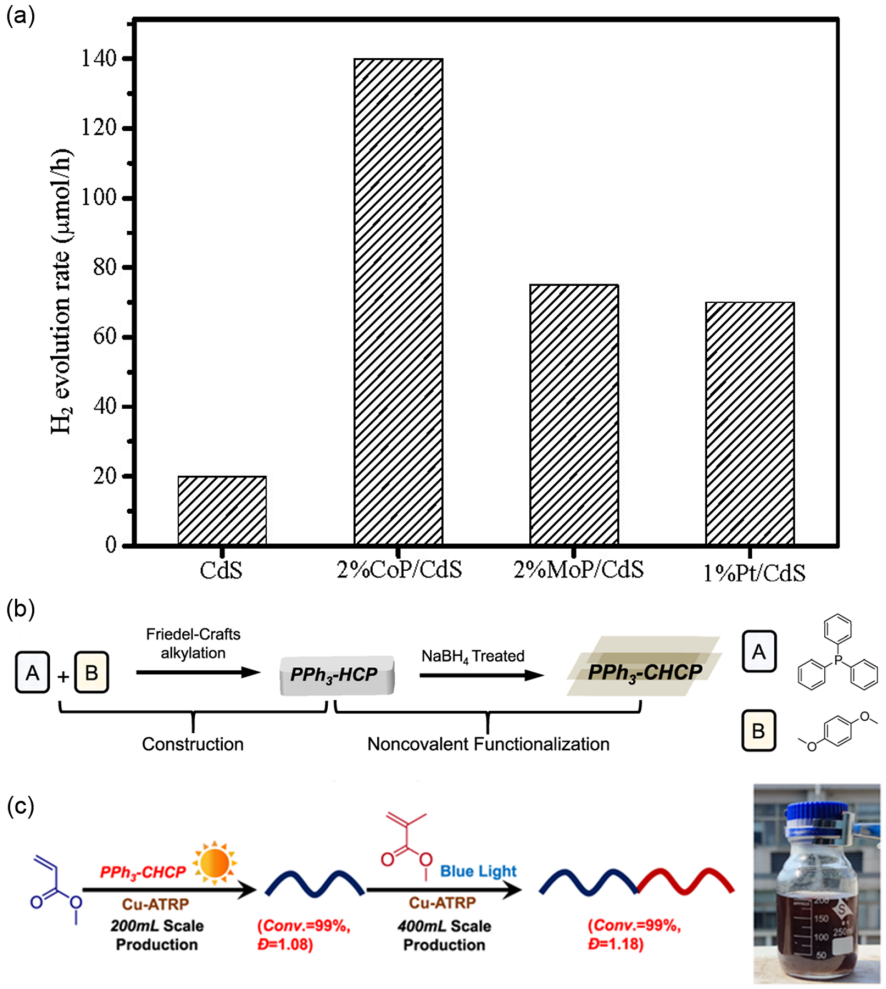

interaction between photocatalytic and Fenton reactions led to a marked increase in catalytic activity, as further confirmed by photocurrent tests and photochemical degradation experiments. Additionally, the Fenton-like process in the Cu_2O/BiOBr system, involving the transition Cu(I)-e^-→Cu(II), plays a crucial role in photocatalytic degradation, with Cu(I) being regenerated through the reducing action of glucose, a widely recognized method for regenerating Fenton catalysts.

In summary, the regeneration of photocatalysts is a key area where the use of photoreduction and chemical reduction strategies allows catalysts such as TNT(Pd)/Fe_2O_3 and Cu_2O/BiOBr to maintain high activity over multiple cycles. The synergistic effect of photocatalysis and Fenton-like reactions further enhances degradation efficiency, offering a promising strategy for the design of robust and sustainable photocatalytic systems. Future research should focus on optimizing these regeneration methods and exploring new materials and mechanisms to further improve the stability and recyclability of photocatalysts.

5. Summary and Outlook

Visible-light photocatalysis has immense application potential and broad development prospects. This review offers a comprehensive exposition of its concept, classification, applications, challenges, and prospects. Delving into its fundamental mechanisms and distinct characteristics, we categorize various photocatalysts for a thorough understanding of the field. Notably, visible-light photocatalysis has demonstrated remarkable performance across multiple applications, including environmental pollution control, organic synthesis chemistry, and energy conversion. However, it faces challenges such as light absorption capability, separation and transport of photogenerated charges, stability, reaction selectivity, and scale-up production. Despite these challenges, the future of visible-light photocatalysis is still promising. This review aims to provide researchers in related fields with a comprehensive and systematic reference to further promote the development of visible-light photocatalysis.

Figure 14

(a) Recycling runs of MO degradation performance of TNT(Pd)/Fe_2O_3 in the presence of H_2O_2 under visible light. (b) The Fe2p XPS of the recovered catalyst of TNT(Pd)/Fe_2O_3. (c) High-resolution XPS spectra for Cu 2p (b) of 15 % Cu_2O/BiOBr before and after four times cycles. (d) Photocatalytic degradation efficiency of MB by 15 % Cu_2O/BiOBr after four times cycles and glucose reduction

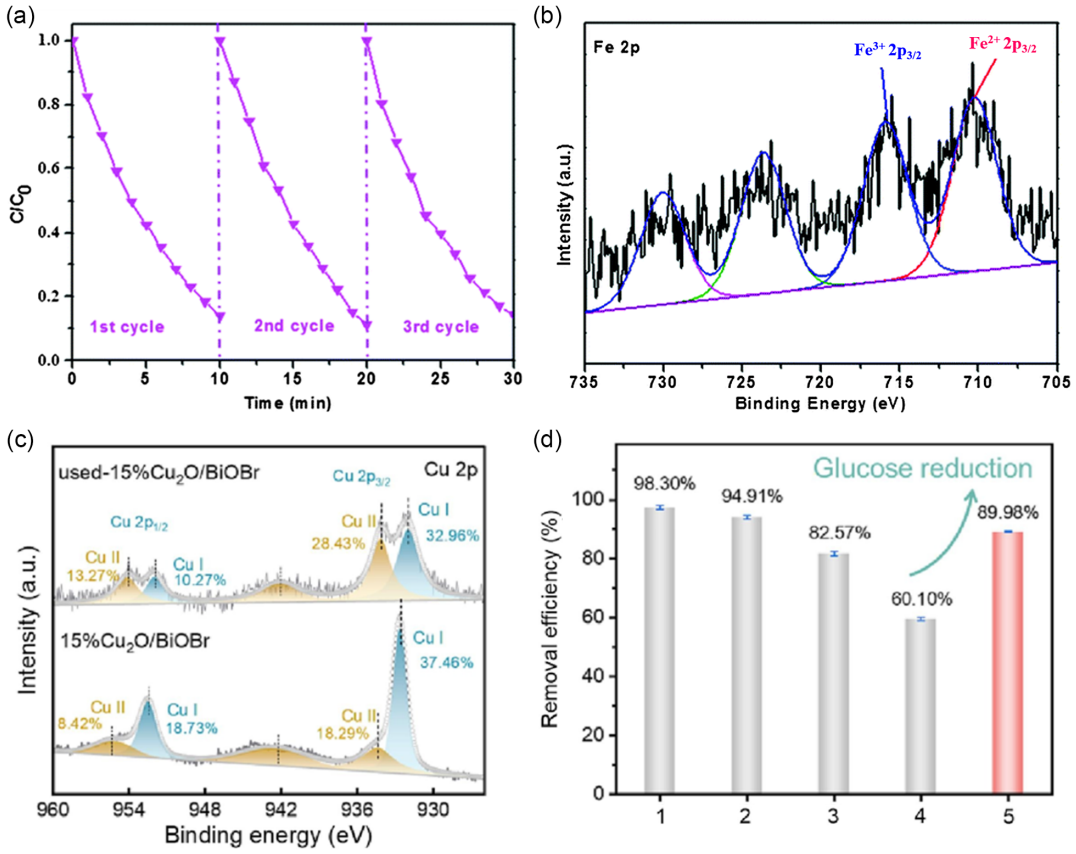

Funding Support

This work was financially supported by the National Natural Science Foundation of China (Grant No. 12104311 and 12004239), the Shanghai Chenguang Program (Grant No. 22CGA74), the National Key R&D Program of China (Grant No. 2021YFB3501700), Shanghai Science and Technology Committee (STCSM) Science and Technology Innovation Program (Grant No. 22N21900400, and 23N21900100), Key R&D Program of Jiangsu Province (Grant No. BE2023048)

Ethical Statement

This study does not contain any studies with human or animal subjects performed by any of the authors.

Conflicts of Interest

The authors declare that they have no conflicts of interest to this work.

Data Availability Statement

Data are available from the corresponding author upon reasonable request.

Author Contribution Statement

Xiaoyang Li: Investigation, Resources, Writing – original draft. **Sihan Lin:** Investigation. **Rongrong Hu:** Conceptualization, Investigation, Resources, Writing – review & editing, Supervision, Funding acquisition. **Pan Liang:** Investigation. **Qiaoyun Wu:** Investigation, Resources. **Bobo Yang:** Investigation. **Shengquan Lin:** Investigation. **Quanlong Xu:** Investigation. **Junnan Mei:** Investigation. **Jun Zou:** Conceptualization, Investigation, Supervision, Funding acquisition.

References

[1] Brunekreef, B., & Holgate, S. T. (2002). Air pollution and health. *The Lancet*, *360*(9341), 1233–1242. https://doi.org/10.1016/S0140-6736(02)11274-8

[2] Si, W., Yang, Z., Wang, X., Lv, Q., Zhao, F., Li, X., . . . , & Huang, C. (2019). Fe, N-codoped graphdiyne displaying efficient oxygen reduction reaction activity. *ChemSusChem*, *12*(1), 173–178. https://doi.org/10.1002/cssc.201802170

[3] Kako, T., Ichihara, F., Liu, G., Meng, X., & Ye, J. (2019). Study on the enhancement of photocatalytic environment purification through ubiquitous-red-clay loading. *SN Applied Sciences*, *1*, 1–8. https://doi.org/10.1007/s42452-018-0149-x

[4] Vaiano, V., & Iervolino, G. (2018). Facile method to immobilize ZnO particles on glass spheres for the

photocatalytic treatment of tannery wastewater. *Journal of Colloid and Interface Science*, *518*, 192–199. https://doi.org/10.1016/j.jcis.2018.02.033

[5] Peng, K., Yu, S., Luo, Y., Zhang, A., Xie, Y., Luo, Y., . . . , & Zhao, J. (2024). Enhancement TiO_2 photocatalytic hydrogen production via using ABO_3 to construct heterojunction. *Colloids and Surfaces A: Physicochemical and Engineering Aspects*, *682*, 132822. https://doi.org/10.1016/j.colsurfa.2023.132822

[6] Fujishima, A., & Honda, K. (1972). Electrochemical photolysis of water at a semiconductor electrode. *Nature*, *238*(5358), 37–38. https://doi.org/10.1038/238037a0

[7] Carey, J. H., Lawrence, J., & Tosine, H. M. (1976). Photodechlorination of PCB's in the presence of titanium dioxide in aqueous suspensions. *Bulletin of Environmental Contamination and Toxicology*, *16*, 697–701. https://doi.org/10.1007/BF01685575

[8] Pruden, A. L., & Ollis, D. F. (1983). Photoassisted heterogeneous catalysis: The degradation of trichloroethylene in water. *Journal of Catalysis*, *82*(2), 404–417. https://doi.org/10.1016/0021-9517(83)90207-5

[9] Song, L., Hu, J., Lu, X., Lu, Z., Xie, J., Hao, A., & Cao, Y. (2022). Boosting the photocatalytic activity and resistance of photostability of ZnS nanoparticles. *Inorganic Chemistry*, *61*(21), 8217–8225. https://doi.org/10.1021/acs.inorgchem.2c00632

[10] Vamvasakis, I., Andreou, E. K., & Armatas, G. S. (2023). Mesoporous dual-semiconductor ZnS/CdS nanocomposites as efficient visible light photocatalysts for hydrogen generation. *Nanomaterials*, *13*(17), 2426. https://doi.org/10.3390/nano13172426

[11] Wei, X., Ou, K., Wang, J., Li, K., Wu, S., Zhang, W., . . . , & Wang, H. (2023). Novel visible light-induced ZnSe/TiO_2 nanorod heterojunction for efficient photocatalysis and degradation of methyl orange. *Journal of Materials Science: Materials in Electronics*, *34*(17), 1339. https://doi.org/10.1007/s10854-023-10764-5

[12] Lin, Y., Cao, Y., Yao, Q., Chai, O. J. H., & Xie, J. (2020). Engineering noble metal nanomaterials for pollutant decomposition. *Industrial & Engineering Chemistry Research*, *59*(47), 20561–20581. https://doi.org/10.1021/acs.iecr.0c04258

[13] Ramírez-Ortega, D., Guerrero-Araque, D., Sierra-Uribe, J. H., Camposeco, R., Gómez, R., & Zanella, R. (2023). Accelerated transfer and separation of charge carriers during the photocatalytic production of hydrogen over Au/ZrO_2–TiO_2 structures by interfacial energy states. *International Journal of Hydrogen Energy*, *48*(42), 15956–15966. https://doi.org/10.1016/j.ijhydene.2023.01.134

[14] Zhu, H., Yuan, X., Yao, Q., & Xie, J. (2021). Shining photocatalysis by gold-based nanomaterials. *Nano Energy*, *88*, 106306. https://doi.org/10.1016/j.nanoen.2021.106306

[15] Konstantinova, E. A., Minnekhanov, A. A., Trusov, G. V., & Kytin, V. G. (2020). Titania-based nanoheterostructured microspheres for prolonged visible-light-driven photocatalysis. *Nanotechnology*, *31*(34), 345207. https://doi.org/10.1088/1361-6528/ab91f1

[16] Chen, S., & Hu, Y. H. (2023). Color TiO_2 materials as emerging catalysts for visible-NIR light photocatalysis, a review. *Catalysis Reviews*, *66*, 1–41. https://doi.org/10.1080/01614940.2023.2169451

[17] Sagadevan, S., Vennila, S., Muthukrishnan, L., Murugan, B., Lett, J. A., Shahid, M. M., . . . , & Johan, M. R. (2020). Improved antimicrobial efficacy and photocatalytic performance of gold decorated titanium dioxide nanohybrid. *Optik*, *224*, 165515. https://doi.org/10.1016/j.ijleo.2020.165515

[18] Ibukun, O., & Jeong, H. K. (2020). Tailoring titanium dioxide by silver particles for photocatalysis. *Current Applied Physics*, *20*(1), 23–28. https://doi.org/10.1016/j.cap.2019.10.009

[19] Chidambaram, S., Baskaran, B., Ganesan, M., Muthusamy, S., Alavandar, S., Muthusamy, S., . . . , & Panchal, H. (2022). One pot synthesis of Ag-Au/ZnO nanocomposites: A multi-junction component for sunlight photocatalysis. *Energy Sources, Part A: Recovery, Utilization, and Environmental Effects*, *44*(1), 758–770. https://doi.org/10.1080/15567036.2022.2050855

[20] Bi, S., Wang, H., Wang, R., & Niu, Z. (2022). Two-dimensional materials for aqueous zinc-ion batteries. *2D Materials*, *9*(4), 042001. https://doi.org/10.1088/2053-1583/ac7e58

[21] Li, T., Huang, H., Wang, S., Mi, Y., & Zhang, Y. (2023). Recent advances in 2D semiconductor nanomaterials for photocatalytic CO_2 reduction. *Nano Research*, *16*(7), 8542–8569. https://doi.org/10.1007/s12274-022-5234-1

[22] Yu, H., Dai, M., Zhang, J., Chen, W., Jin, Q., Wang, S., & He, Z. (2023). Interface engineering in 2D/2D heterogeneous photocatalysts. *Small*, *19*(5), 2205767. https://doi.org/10.1002/smll.202205767

[23] Zhu, B., Cheng, B., Fan, J., Ho, W., & Yu, J. (2021). g-C_3N_4-based 2D/2D composite heterojunction photocatalyst. *Small Structures*, *2*(12), 2100086. https://doi.org/10.1002/sstr.202100086

[24] Rana, S., Kumar, A., Sharma, G., Dhiman, P., García-Penas, A., & Stadler, F. J. (2023). Recent advances in perovskite-based Z-scheme and S-scheme heterojunctions for photocatalytic CO_2 reduction. *Chemosphere*, *339*, 139765. https://doi.org/10.1016/j.chemosphere.2023.139765

[25] Mei, J., Liao, T., & Sun, Z. (2022). 2D/2D heterostructures: Rational design for advanced batteries and electrocatalysis. *Energy & Environmental Materials*, *5*(1), 115–132. https://doi.org/10.1002/eem2.12184

[26] Sun, X., Deng, H., Zhu, W., Yu, Z., Wu, C., & Xie, Y. (2016). Interface engineering in two-dimensional heterostructures: Towards an advanced catalyst for Ullmann couplings. *Angewandte Chemie International Edition*, *55*(5), 1704–1709. https://doi.org/10.1002/anie.201508571

[27] Nicks, J., Sasitharan, K., Prasad, R. R., Ashworth, D. J., & Foster, J. A. (2021). Metal-organic framework nanosheets: Programmable 2D materials for catalysis, sensing, electronics, and separation applications. *Advanced Functional Materials*, *31*(42), 2103723. https://doi.org/10.1002/adfm.202103723

[28] Zhang, Y., Zou, K., Gao, Z., Ma, Y., Xu, L., Lu, F., . . . , & Luo, F. (2023). Large negative magnetoresistance in all-2D-materials-based spin valves. *physica status solidi (RRL)–Rapid Research Letters*, *17*(7), 2300073. https://doi.org/10.1002/pssr.202300073

[29] Alomar, M., Liu, Y., Chen, W., & Fida, H. (2019). Controlling the growth of ultrathin MoS_2 nanosheets/CdS nanoparticles by two-step solvothermal synthesis for enhancing photocatalytic activities under visible light. *Applied Surface Science*, *480*, 1078–1088. https://doi.org/10.1016/j.apsusc.2019.03.014

[30] Wen, Y., Wang, D., Li, H., Jiang, W., Zhou, T., Deng, X., . . . , & Che, G. (2021). Enhanced photocatalytic hydrogen evolution of 2D/2D N-Sn_3O_4/g-C_3N_4 S-scheme heterojunction under visible light irradiation. *Applied Surface Science*, *567*, 150903. https://doi.org/10.1016/j.apsusc.2021.150903

[31] Wu, J., Li, L., Li, X. A., Min, X., & Xing, Y. (2022). A novel 2D graphene oxide modified α-$AgVO_3$ nanorods: Design, fabrication, and enhanced visible-light photocatalytic performance. *Journal of Advanced Ceramics*, *11*, 308–320. https://doi.org/10.1007/s40145-021-0534-6

[32] Yuan, Y. J., Lu, N., Bao, L., Tang, R., Zhang, F. G., Guan, J., . . . , & Zou, Z. (2022). SiP nanosheets: A metal-free two-dimensional photocatalyst for visible-light photocatalytic H_2 production and nitrogen fixation. *ACS Nano*, *16*(8), 12174–12184. https://doi.org/10.1021/acsnano.2c02831

[33] Zhang, Y., Wang, Y., Xu, W., Wu, Y., Zeng, C., Wang, Y., . . . , & Yang, R. (2022). Increased solar absorption and promoted photocarrier separation in atomically thin 2D carbon nitride sheets for enhanced visible-light photocatalysis. *Chemical Engineering Journal*, *431*, 133219. https://doi.org/10.1016/j.cej.2021.133219

[34] Qiu, L., Qiu, X., Li, P., Ma, M., Chen, X., & Duo, S. (2020). In-situ self-assembly synthesis of 2D/2D CdS/g-C_3N_4 heterojunction for efficient visible-light photocatalytic performance. *Materials Letters*, *268*, 127566. https://doi.org/10.1016/j.matlet.2020.127566

[35] Mallikarjuna, K., & Kim, H. (2021). Bandgap-tuned ultra-small SnO_2-nanoparticle-decorated 2D-Bi_2WO_6 nanoplates for visible-light-driven photocatalytic applications. *Chemosphere*, *263*, 128185. https://doi.org/10.1016/j.chemosphere.2020.128185

[36] Zhou, M., Huang, W., Zhao, Y., Jin, Z., Hua, X., Li, K., . . . , & Cai, Z. (2020). 2D gC_3N_4/BiOBr heterojunctions with enhanced visible light photocatalytic activity. *Journal of Nanoparticle Research*, *22*, 1–11. https://doi.org/10.1007/s11051-019-4739-3

[37] Qiu, J., Wu, M., Yu, L., Li, J., Di, J., Zhang, S., . . . , & Wu, Z. (2020). Vanadate-Rich BiOBr/Bi nanosheets for effective adsorption and visible-light-driven photodegradation of rhodamine B. *Journal of Nanoscience and Nanotechnology*, *20*(4), 2267–2276. https://doi.org/10.1166/jnn.2020.17331

[38] Sahoo, D., Shakya, J., Ali, N., Yoo, W. J., & Kaviraj, B. (2022). Edge rich ultrathin layered MoS_2 nanostructures for superior visible light photocatalytic activity. *Langmuir*, *38*(4), 1578–1588. https://doi.org/10.1021/acs.langmuir.1c03013

[39] Li, M., Chen, M., Lee, S. L. J., & Lin, S. (2023). Facile fabrication of a 2D/2D CoFe-LDH/g-C_3N_4 nanocomposite with enhanced photocatalytic tetracycline degradation. *Environmental Science and Pollution Research*, *30*(2), 4709–4720. https://doi.org/10.1007/s11356-022-22554-3

[40] Zhang, Y., Xu, J., Mei, J., Sarina, S., Wu, Z., Liao, T., . . . , & Sun, Z. (2020). Strongly interfacial-coupled 2D-2D TiO_2/g-C_3N_4 heterostructure for enhanced visible-light induced synthesis and conversion. *Journal of Hazardous Materials*, *394*, 122529. https://doi.org/10.1016/j.jhazmat.2020.122529

[41] Tang, Q. Y., Yang, M. J., Yang, S. Y., & Xu, Y. H. (2021). Enhanced photocatalytic degradation of glyphosate over 2D CoS/BiOBr heterojunctions under visible light irradiation. *Journal of Hazardous Materials*, *407*, 124798. https://doi.org/10.1016/j.jhazmat.2020.124798

[42] Majumdar, A., Ghosh, U., & Pal, A. (2021). Novel 2D/2D g-C_3N_4/Bi_4NbO_8Cl nano-composite for enhanced photocatalytic degradation of oxytetracycline under visible LED light irradiation. *Journal of Colloid and Interface Science*, *584*, 320–331. https://doi.org/10.1016/j.jcis.2020.09.101

[43] Marin, M. L., Santos-Juanes, L., Arques, A., Amat, A. M., & Miranda, M. A. (2012). Organic photocatalysts for the oxidation of pollutants and model compounds. *Chemical Reviews*, *112*(3), 1710–1750. https://doi.org/10.1021/cr2000543

[44] Fagnoni, M., Dondi, D., Ravelli, D., & Albini, A. (2007). Photocatalysis for the formation of the C-C bond. *Chemical Reviews*, *107*(6), 2725–2756. https://doi.org/10.1021/cr068352x

[45] Yang, M. Q., Zhang, N., Wang, Y., & Xu, Y. J. (2017). Metal-free, robust, and regenerable 3D graphene–organics aerogel with high and stable photosensitization efficiency. *Journal of Catalysis*, *346*, 21–29. https://doi.org/10.1016/j.jcat.2016.11.012

[46] Xu, Q., Li, E., Zhao, R., Liang, T., Zhang, H., Hu, W., & Zhang, N. (2020). Preparation of organic porous materials-TiO_2/Cu composite with excellent photocatalytic degradation performances toward degradation of organic pollutants in wastewater. *Journal of Polymer Research*, *27*, 1–8. https://doi.org/10.1007/s10965-020-02163-9

[47] Li, X., Li, Y., Huang, Y., Zhang, T., Liu, Y., Yang, B., . . . , & Zhang, J. (2017). Organic sponge photocatalysis. *Green Chemistry*, *19*(13), 2925–2930. https://doi.org/10.1039/C6GC03558B

[48] Jin, S., Han, C., Xiang, S., Zhang, C., & Jiang, J. X. (2023). Furan-based conjugated polymer photocatalysts for highly active photocatalytic hydrogen evolution under visible light. *Journal of Catalysis*, *427*, 115091. https://doi.org/10.1016/j.jcat.2023.08.007

[49] Wang, Z., Liu, H., Lei, Z., Huang, L., Wu, T., Liu, S., . . . , & Wang, X. (2020). Graphene aerogel for photocatalysis-assist uranium elimination under visible light and air atmosphere. *Chemical Engineering Journal*, *402*, 126256. https://doi.org/10.1016/j.cej.2020.126256

[50] Mohsin, M., Bhatti, I. A., Ashar, A., Khan, M. W., Farooq, M. U., Khan, H., . . . , & Mahmood, N. (2021). Iron-doped zinc oxide for photocatalyzed degradation of humic acid from municipal wastewater. *Applied Materials Today*, *23*, 101047. https://doi.org/10.1016/j.apmt.2021.101047

[51] Zhou, Y., Elchalakani, M., Liu, H., Briseghella, B., & Sun, C. (2022). Photocatalytic concrete for degrading organic dyes in water. *Environmental Science and Pollution Research*, *29*(26), 39027–39040. https://doi.org/10.1007/s11356-021-18332-2

[52] He, X., Zhu, J., Tan, L., Wang, H., & Zhou, M. (2020). Visible light-induced photocatalytic degradation of gaseous toluene by Ce, S and N doped ionic liquid-TiO_2. *Materials Science in Semiconductor Processing*, *120*, 105259. https://doi.org/10.1016/j.mssp.2020.105259

[53] Wu, F., Liu, Y., Chen, X., Han, J., Hu, D., Wang, W., & Wang, S. (2024). Dual Z-scheme ternary heterojunction photocatalyst with enhanced visible-light photocatalytic degradation of organic pollutants. *Journal of the Chinese Chemical Society*, *71*(1), 35–44. https://doi.org/10.1002/jccs.202300373

[54] Pirsaheb, M., Hossaini, H., Fatahi, N., Jafari, Z., Jafari, F., & Motlagh, R. J. (2023). The visible-light photocatalytic degradation of ibuprofen by the CuS-Fe_3O_4/RGO catalyst. *Inorganic Chemistry Communications*, *158*, 111597. https://doi.org/10.1016/j.inoche.2023.111597

[55] Shee, N. K., & Kim, H. J. (2023). Surface modification of ZnO with Sn (IV)-porphyrin for enhanced visible light photocatalytic degradation of amaranth dye. *Molecules*, *28*(18), 6481. https://doi.org/10.3390/molecules28186481

[56] Shi, X., Liu, B., Meng, G., Wu, P., Lian, J., Kong, W., & Liu, R. (2024). Enhanced visible-light photocatalytic degradation of oxytetracycline hydrochloride by Z-scheme CuO/Bi_2WO_6 heterojunction. *Journal of Alloys and Compounds*, *1002*, 175219. https://doi.org/10.1016/j.jallcom.2024.175219

[57] Seling, T. R., Shringi, A. K., Wang, K., Riaz, U., & Yan, F. (2024). Bi_2O_2S nanosheets for effective visible light photocatalysis of anionic dye degradation. *Materials Letters*, *361*, 136136. https://doi.org/10.1016/j.matlet.2024.136136

[58] Panahi, P. N., & Niko, A. (2024). Visible light photocatalytic degradation of several VOCs (Ethyl Acetate, 2-Propanol, and Benzene) over a graphene/ZnO composite. *Journal of*

Electronic Materials, *53*, 4706–4714. https://doi.org/10.1007/s11664-024-11175-w

[59] Giousis, T., Fang, S., Miola, M., Li, S., Lazanas, A., Prodromidis, M., ..., & Pescarmona, P. P. (2023). Germanane and butyl-functionalized germanane as visible-light photocatalysts for the degradation of water pollutants. *Journal of Environmental Chemical Engineering*, *11*(3), 109784. https://doi.org/10.1016/j.jece.2023.109784

[60] Lahootifar, Z., Habibi-Yangjeh, A., Rahim Pouran, S., & Khataee, A. (2023). G-C_3N_4 dots decorated with hetaerolite: Visible-light photocatalyst for degradation of organic contaminants. *Catalysts*, *13*(2), 346. https://doi.org/10.3390/catal13020346

[61] Chen, H., Hu, Y., Ying, Z., Xia, Y., Ye, J., Zhao, J., & Zhang, S. (2023). BiOI-SnO_2 heterojunction design to boost visible-light-driven photocatalytic NO purification. *International Journal of Environmental Research and Public Health*, *20*(5), 4009. https://doi.org/10.3390/ijerph20054009

[62] Yedase, G. S., Kumar, S., Stahl, J., König, B., & Yatham, V. R. (2021). Cerium-photocatalyzed aerobic oxidation of benzylic alcohols to aldehydes and ketones. *Beilstein Journal of Organic Chemistry*, *17*(1), 1727–1732. https://doi.org/10.3762/bjoc.17.121

[63] Tambe, S. D., & Cho, E. J. (2022). Organophotocatalytic oxidation of alcohols to carboxylic acids. *Bulletin of the Korean Chemical Society*, *43*(11), 1226–1230. https://doi.org/10.1002/bkcs.12610

[64] Zhang, G., Wang, K., Zhang, D., Zhang, C., Tan, W., Chen, Z., & Chen, F. (2023). Decarboxylative allylation of silanecarboxylic acids enabled by organophotocatalysis. *Organic Letters*, *25*(40), 7406–7411. https://doi.org/10.1021/acs.orglett.3c02907

[65] Xiang, Q., Yu, J., & Jaroniec, M. (2011). Preparation and enhanced visible-light photocatalytic H_2-production activity of graphene/C_3N_4 composites. *The Journal of Physical Chemistry C*, *115*(15), 7355–7363. https://doi.org/10.1021/jp200953k

[66] Lu, C., Du, S., Zhao, Y., Wang, Q., Ren, K., Li, C., & Dou, W. (2021). Efficient visible-light photocatalytic H_2 evolution with heterostructured Ag_2S modified CdS nanowires. *RSC Advances*, *11*(45), 28211–28222. https://doi.org/10.1039/D1RA04823F

[67] Guan, W., Jia, R., Zhang, L., Meng, M., Wang, P., Wang, Y., ..., & Yu, L. (2023). Construction of $PdSe_2$/$ZnIn_2S_4$ heterojunctions with covalent interface for highly efficient photocatalytic hydrogen evolution. *Journal of Colloid and Interface Science*, *649*, 685–693. https://doi.org/10.1016/j.jcis.2023.06.130

[68] Huang, Q., Yang, J., Qi, F., Zhang, W., Zhang, N., Liang, Z., ..., & Huo, B. (2022). Visible light driven photocatalytic reduction of CO_2 on Au-Pt/Cu_2O/ReS_2 with high efficiency and controllable selectivity. *Chemical Engineering Journal*, *437*, 135299. https://doi.org/10.1016/j.cej.2022.135299

[69] Tian, C., Li, C., Zhao, C., Liu, D., & He, X. (2023). A novel synthetic 3D interconnected porous carbon-rich graphitic carbon nitride for boosting visible light photocatalytic hydrogen production and dye contaminant degradation. *Catalysts*, *13*(10), 1345. https://doi.org/10.3390/catal13101345

[70] Yang, Y., Lu, C., Ren, J., Li, X., Ma, Y., Huang, W., & Zhao, X. (2020). Enhanced photocatalytic hydrogen evolution over TiO_2/g-C_3N_4 2D heterojunction coupled with plasmon Ag nanoparticles. *Ceramics International*, *46*(5), 5725–5732. https://doi.org/10.1016/j.ceramint.2019.11.021

[71] Li, J., Yuan, C., Liu, X., Zhang, T., Su, K., Xu, J., ..., & Rao, G. (2023). Solar photocatalytic hydrogen production of g-C_3N_4/$KTaO_3$ heterojunction for water splitting via interface engineering. *Journal of Materials Science: Materials in Electronics*, *34*(12), 1067. https://doi.org/10.1007/s10854-023-10460-4

[72] Liu, Y., Jiang, L., Tian, Y., Xu, Z., Wang, W., Qiu, M., ..., & Wang, Y. (2023). Covalent organic framework/g-C_3N_4 van der Waals heterojunction toward H_2 production. *Inorganic Chemistry*, *62*(7), 3271–3277. https://doi.org/10.1021/acs.inorgchem.2c04366

[73] Li, S., Yang, Y., Wan, S., Wang, R., Yu, M., Song, F., & Zhong, Q. (2023). Supramolecular self-assemble deficient carbon nitride nanotubes for efficient photocatalytic CO_2 reduction. *Journal of Colloid and Interface Science*, *651*, 726–733. https://doi.org/10.1016/j.jcis.2023.08.042

[74] Li, Q., He, L., Zeng, Y., Zhao, Y., & Ding, M. (2023). CdS-assisted ultrathin porous nitrogen-vacancy carbon nitride nanosheets for visible-light photocatalytic CO_2 reduction. *Carbon*, *214*, 118384. https://doi.org/10.1016/j.carbon.2023.118384

[75] Liu, J., Du, T., Chen, P., Yue, Q., Wang, H., Zhou, L., & Wang, Y. (2024). Construction of Bi_2WO_6/g-C_3N_4/Cu foam as 3D Z-scheme photocatalyst for photocatalytic CO_2 reduction. *Applied Surface Science*, *664*, 160274. https://doi.org/10.1016/j.apsusc.2024.160274

[76] Zheng, Z., Du, T., Chen, P., Yue, Q., Wang, H., Zhou, L., & Wang, Y. (2024). 2D/1D nested hollow porous $ZnIn_2S_4$/g-C_3N_4 heterojunction based on morphology modulation for photocatalytic CO_2 reduction. *Journal of Environmental Chemical Engineering*, *12*(3), 112971. https://doi.org/10.1016/j.jece.2024.112971

[77] Arora, I., Chawla, H., Chandra, A., Sagadevan, S., & Garg, S. (2022). Advances in the strategies for enhancing the photocatalytic activity of TiO_2: Conversion from UV-light active to visible-light active photocatalyst. *Inorganic Chemistry Communications*, *143*, 109700. https://doi.org/10.1016/j.inoche.2022.109700

[78] Ren, Y., Zhu, Y., Gao, S., Liu, X., Li, H., & Rui, S. (2024). Preparation of HC/BiOCl composite photocatalyst and its visible photocatalytic performance. *Inorganic Chemistry Communications*, *163*, 112329. https://doi.org/10.1016/j.inoche.2024.112329

[79] Chen, Z., Tang, T., Ni, B., Bai, M., Qi, Y., Yang, X., ..., & Lin, J. (2023). Amorphous TiO_2 doped with carbon for visible light photocatalytic oxidation of elemental mercury. *Chemical Physics Letters*, *831*, 140860. https://doi.org/10.1016/j.cplett.2023.140860

[80] Yuan, Y., Wang, W. L., Wang, Z. W., Wang, J., & Wu, Q. Y. (2024). Single-atom Ag-loaded carbon nitride photocatalysts for efficient degradation of acetaminophen: The role of Ag-atom and O_2. *Journal of Environmental Sciences*, *139*, 12–22. https://doi.org/10.1016/j.jes.2023.03.042

[81] Gan, Z., Wu, X., Meng, M., Zhu, X., Yang, L., & Chu, P. K. (2014). Photothermal contribution to enhanced photocatalytic performance of graphene-based nanocomposites. *ACS Nano*, *8*(9), 9304–9310. https://doi.org/10.1021/nn503249c

[82] Gui, X., Zhou, Y., Pan, D., Li, H., Wang, Y., Liang, Q., ..., & Li, Z. (2024). Construction of ternary Ni_2P/ZIF-8/CdS composite for efficient photocatalytic hydrogen production and pollutant degradation: Accelerating separation of photogenerated carriers. *Journal of Physics and Chemistry of Solids*, *190*, 111983. https://doi.org/10.1016/j.jpcs.2024.111983

[83] Meng, M., Yang, L., Yang, J., Zhu, Y., Li, C., Xia, H., ..., & Gan, Z. (2023). Two-dimensional lateral anatase-rutile TiO_2 phase junctions with oxygen vacancies for robust photoelectrochemical water splitting. *Journal of Colloid and Interface Science*, *648*, 56–65. https://doi.org/10.1016/j.jcis.2023.05.193

[84] Liu, L., Liu, J., & Sun, D. D. (2012). Graphene oxide enwrapped Ag_3PO_4 composite: Towards a highly efficient

and stable visible-light-induced photocatalyst for water purification. *Catalysis Science & Technology*, *2*(12), 2525–2532. https://doi.org/10.1039/C2CY20483E

[85] Dong, P., Wang, Y., Cao, B., Xin, S., Guo, L., Zhang, J., & Li, F. (2013). Ag_3PO_4/reduced graphite oxide sheets nanocomposites with highly enhanced visible light photocatalytic activity and stability. *Applied Catalysis B: Environmental*, *132*, 45–53. https://doi.org/10.1016/j.apcatb.2012.11.022

[86] Lewandowski, Ł., Zwara, J., Gołąbiewska, A., Klimczuk, T., Trykowski, G., & Zaleska-Medynska, A. (2022). New approach for the synthesis of Ag_3PO_4-graphene photocatalysts. *Materials Science in Semiconductor Processing*, *149*, 106851. https://doi.org/10.1016/j.mssp.2022.106851

[87] Mohammed, M. K. (2020). Carbon nanotubes loaded ZnO/Ag ternary nanohybrid with improved visible light photocatalytic activity and stability. *Optik*, *217*, 164867. https://doi.org/10.1016/j.ijleo.2020.164867

[88] Su, F., Mathew, S. C., Lipner, G., Fu, X., Antonietti, M., Blechert, S., & Wang, X. (2010). mpg-C_3N_4-catalyzed selective oxidation of alcohols using O_2 and visible light. *Journal of the American Chemical Society*, *132*(46), 16299–16301. https://doi.org/10.1021/ja102866p

[89] Bao, X., Lv, X., Wang, Z., Wang, M., Liu, M., Dai, D., . . . , & Huang, B. (2021). Nitrogen vacancy enhanced photocatalytic selective oxidation of benzyl alcohol in g-C_3N_4. *International Journal of Hydrogen Energy*, *46*(76), 37782–37791. https://doi.org/10.1016/j.ijhydene.2021.09.052

[90] Fu, M. C., Shang, R., Zhao, B., Wang, B., & Fu, Y. (2019). Photocatalytic decarboxylative alkylations mediated by triphenylphosphine and sodium iodide. *Science*, *363*(6434), 1429–1434. https://doi.org/10.1126/science.aav3200

[91] Ma, B., Zhang, R., Lin, K., Liu, H., Wang, X., Liu, W., & Zhan, H. (2018). Large-scale synthesis of noble-metal-free phosphide/CdS composite photocatalysts for enhanced H_2 evolution under visible light irradiation. *Chinese Journal of Catalysis*, *39*(3), 527–533. https://doi.org/10.1016/S1872-2067(17)62931-0

[92] Fang, W. W., Yang, G. Y., Fan, Z. H., Chen, Z. C., Hu, X. L., Zhan, Z., . . . , & Tan, B. E. (2023). Conjugated cross-linked phosphine as broadband light or sunlight-driven photocatalyst for large-scale atom transfer radical polymerization. *Nature Communications*, *14*(1), 2891. https://doi.org/10.1038/s41467-023-38402-y

[93] Peng, Q., Peng, G., Wu, L., Chen, Y., Han, B., Su, Q., . . . , & Li, X. (2020). Photo-reduction enables catalyst regeneration in Fenton reaction on an Fe_2O_3-decorated TiO_2 nanotube-based photocatalyst. *Dalton Transactions*, *49*(20), 6730–6737. https://doi.org/10.1039/D0DT00670J

[94] Gao, M., Li, W., Su, X., Li, Z., Ding, X., Du, X., . . . , & Wei, T. (2023). A regenerable Cu_2O/BiOBr S-scheme heterojunction photocatalysts for efficient photocatalytic degradation of mixed organic pollutants. *Separation and Purification Technology*, *313*, 123447. https://doi.org/10.1016/j.seppur.2023.123447

How to Cite: Li, X., Lin, S., Hu, R., Liang, P., Wu, Q., Yang, B., . . . , & Zou, J. (2025). Recent Progress in Visible-Light Photocatalysts Materials: Synthesis, Applications, Challenges, and Prospects. *Journal of Optics and Photonics Research*. https://doi.org/10.47852/bonviewJOPR52023222